HAND-TREMOR FREQUENCY ESTIMATION IN VIDEOS

by

Jian Zheng

in partial fulfillment of the requirements for the degree of

Master of Science
in Embedded Systems

at the Delft University of Technology,
to be defended publicly on Wednesday August 22, 2018 at 13:00 PM.

Student number:	4587472	
Thesis committee:	Prof. Dr. Reinders,	TU Delft
	Dr. J. C. van Gemert,	TU Delft
	Dr. Silvia Pintea,	TU Delft
	Dr. Zeki Erkin,	TU Delft

An electronic version of this thesis is available at http://repository.tudelft.nl/.

TU Delft Delft University of Technology

PREFACE

This report mainly contains two parts of my MSc thesis, a scientific paper and a supplemental document. The scientific paper is the main part which includes the introduction, related work, methodology, experiments and a conclusion of this research project. While the supplemental document contains additional material that provides the background and more details of the research. It covers a discussion about challenges and proposed methods, preliminary knowledge for understanding mentioned techniques in the scientific paper, and supplements for the experiment.

I would like to express my great appreciation to my thesis advisor Dr. Jan van Gemert for providing me the opportunity to do an MSc thesis on the exciting topic of computer vision, for the valuable advice during my work. Also, I would like to offer my special thanks to my daily supervisor Dr. Silvia Pintea. Her extraordinary motivation and support has been of great importance and has been very much appreciated.

I also want to thank my beloved friends and family that have always been standing by my side, I would like to let you know that your support and encouragement was worth more than I can express on paper.

Thank you.

Jian Zheng
Delft, August 2018

1

Scientific Paper

Hand-Tremor Frequency Estimation in Videos

Jian Zheng
Vision Lab, Delft University of Technology
Delft, Netherlands
J.zheng-2@student.tudelft.nl

Abstract

We focus on the problem of estimating human hand-tremor frequency from input RGB video data. Estimating tremors from video is important for non-invasive monitoring, analyzing and diagnosing patients suffering from motor-disorders such as Parkinson's disease. We consider two approaches for hand-tremor frequency estimation: (a) a Lagrangian approach where we detect the hand at every frame in the video, and estimate the tremor frequency along the trajectory; and (b) an Eulerian approach where we first localize the hand, we subsequently remove the large motion along the movement trajectory of the hand, and we use the video information over time encoded as intensity values or phase information to estimate the tremor frequency. We estimate hand tremors on a new human tremor dataset, TIM-Tremor*, containing 55 tremor patient recordings together with: associated ground truth accelerometer data from the most affected hand, RGB video data, and aligned depth data, as well as a multitude of more dynamic tasks, involving larger motion of the hands.*

1. Introduction

We focus on human hand-tremor frequency estimation from videos captured with common consumer RGB cameras. The problem has a considerable importance in medical applications for aiding the medical personnel in the task of motor-disorder patient monitoring and tremor diagnosing [7, 13, 26, 34]. Traditionally the clinical practice uses body-worn accelerometers which offer excellent measurements, yet is intrusive, slow to setup, and allows only measuring a single location per accelerometer. Replacing accelerometers with a common RGB camera offers a non-intrusive method of measuring full-body tremors, offering a strong advantage in the clinical practice.

In the context of tremor analysis, existing approaches require the use of specialized sensors [5, 8, 14, 15], which makes it difficult to apply these methods in practice. Moreover, the targeted application of these approaches are the more high-level tremor diagnosing problem [14, 27] or tremor/no-tremor classification [29]. We propose to estimate human hand-tremor frequency from RGB videos, and compare against ground truth accelerometer data.

The main challenge, when performing human tremor frequency estimation, is the current lack of openly available realistic datasets. Existing work on human tremor analysis either evaluates using in-house data that is not publicly available [5, 14, 37], or on simulated tremor data where no ground truth tremor statistics are provided [29]. This limits the assessment of human tremor analysis methods and thus its progress. An open evaluation dataset is needed.

In this work: (i) we evaluate the frequency of human hand-tremors from RGB videos and we analyze two possible approaches: (i.a) a Lagrangian approach that focuses on the motion of the hand in the image plane and estimate tremor over the hand positions; (i.b) an Eulerian approach that aligns the hand position over a temporal window, by tracking it, and subsequently uses the image information over time as extracted from intensity values and phase-images, to perform a windowed Fourier analysis at every hand pixel; (ii) we bring forth the *TIM-Tremor* dataset, which will be made publicly available, containing: 55 RGB patient videos, together with associated ground-truth accelerometer recordings on the most affected hand, as well as aligned depth-data; (iii) we analyze two variants of the Lagrangian approach and two variants of the Eulerian approach and evaluate them numerically on our proposed *TIM-Tremor* human tremor dataset.

2. Related work

2.1. Motion analysis

Periodic motion. The work in [23] performs action recognition by using space-time repetitive motion templates. Similar to using templates, in [4] a self-similarity relying on time-frequency analysis is used for action recognition. The work in [12] performs a spectral decomposition of moving objects to encode periodic motions for object recognition, while [30] performs eigen decomposition and describes pe-

riodic motion by the circularity or toroidality of an associated geometric space. Following a similar trend, in [19] complex motion is decomposed into a sequence of simple linear dynamic models for motion categorization. The work in [25] focuses on pedestrian detection through periodic movement analysis. Similar to us, the work in [29] performs tremor analysis, however in [29] videos are classified into tremor /no-tremor using optical flow features and SVM. In this work we also focus on periodic motion analysis, however our end goal is tremor frequency estimation rather than action recognition, object tracking or recognition.

Differently, in [18, 28, 33] deep network architectures are trained for counting action repetitions. These actions must be clearly visible and recognizable in the camera view for the deep network architectures to work, while we focus on tremors which are subtle motions.

The most similar work to our work is the work performed in [31, 32] where tremor frequency is measure from pixel intensities in the video. However these methods assumes the location of the body part at which the tremor is measured to be known in advance and moreover, the frequency is estimated over intensity values rather than detected hand location over time, or image phase-information over time, as we propose here. The authors do not provide either code or data, which makes it impossible for us to compare with their approach.

Subtle motion. Small motion, difficult to see with the bare eyes, can be magnified [17, 35] through a complex steerable pyramid. In the more realistic case, when the subtle motion is combined with a large motion, follow up work can magnify subtle motions such as tremors in the presence of large object motion such as walking [9, 39]. Video frequency analysis has been also employed for estimating the properties of physical materials [6]. We also employ signal analysis in the Fourier domain, however rather than magnifying the subtle motion or estimating material properties, we estimate the frequency of the subtle tremor motion. The works in [14, 15] use specialized sensors or digital light-processing projector and a high frame-rate camera to detect small vibrations. Unlike [14, 15], we do not employ specific cameras or expensive sensors, we estimate the tremor frequency from common RGB videos.

2.2. Human body pose estimation

Works such as [2, 22] perform body pose estimation over multiple people, in deep networks. In [2, 3, 24, 36] cascaded prediction or iterative optimizations are used for body pose estimation. We use the method in [36] for estimating where to measure the tremors. We opt for [36] due to its ease of usage and robustness. In this work we use the MPII Human Body Pose dataset [1] for training the human body pose estimation models.

3. Hand-tremor frequency estimation

We start by localizing the affected hand. Subsequently, we consider two methods for hand-tremor frequency estimation: (a) Lagrangian hand-tremor frequency estimation, and (b) Eulerian hand-tremor frequency estimation.

3.1. Hand location estimation

A first step in estimating human hand-tremors, is localizing the affected hand. For this, we use the robust human body pose estimation proposed in [36]. This method provides us a hand location per frame (x_i, y_i). We perform the tremor analysis on shorter temporal windows of the video, $w(t)$.

3.2. (a) Lagrangian hand-tremor frequency estimation

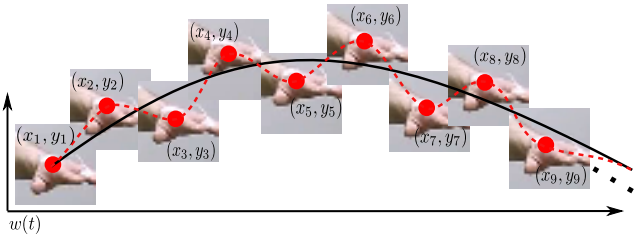

Figure 1: Lagrangian hand-tremor estimation is based on frequency estimation of (x, y) coordinates. We detect the hand position $(x_i, y_i)_{i \in w(t)}$ at every frame i over a temporal window $w(t)$. The hand motion is characterized by a large motion, depicted by the black line, and a small motion, depicted by the red dotted line. We smooth this information over time, using a Kalman tracker to obtain the smooth coordinates of the hand.

Figure 1 depicts the idea behind the Lagrangian hand-tremor frequency estimation. We start by detecting the hand locations $(x_i, y_i)_{i \in w(t)}$ over the temporal window $w(t)$. The hand motion is typically characterized by a combination of two motions: a large hand trajectory motion, depicted through the continuous black line, and a small motion corresponding to the tremor, depicted in Figure 1 by the dotted red line. We first apply a Kalman-filter tracker [38] to the initial hand locations, detected by pose estimation algorithm [36]. This step is used for smoothing the hand trajectory, to obtain the large hand motion. We subsequently subtract this smooth trajectory from the original hand locations to retain only the *x and y locations* of the small hand motion, corresponding to the tremor. Thereafter, we apply the windowed Fourier transform over these corrected locations. This provides us a PSD (Power Spectrum Density)

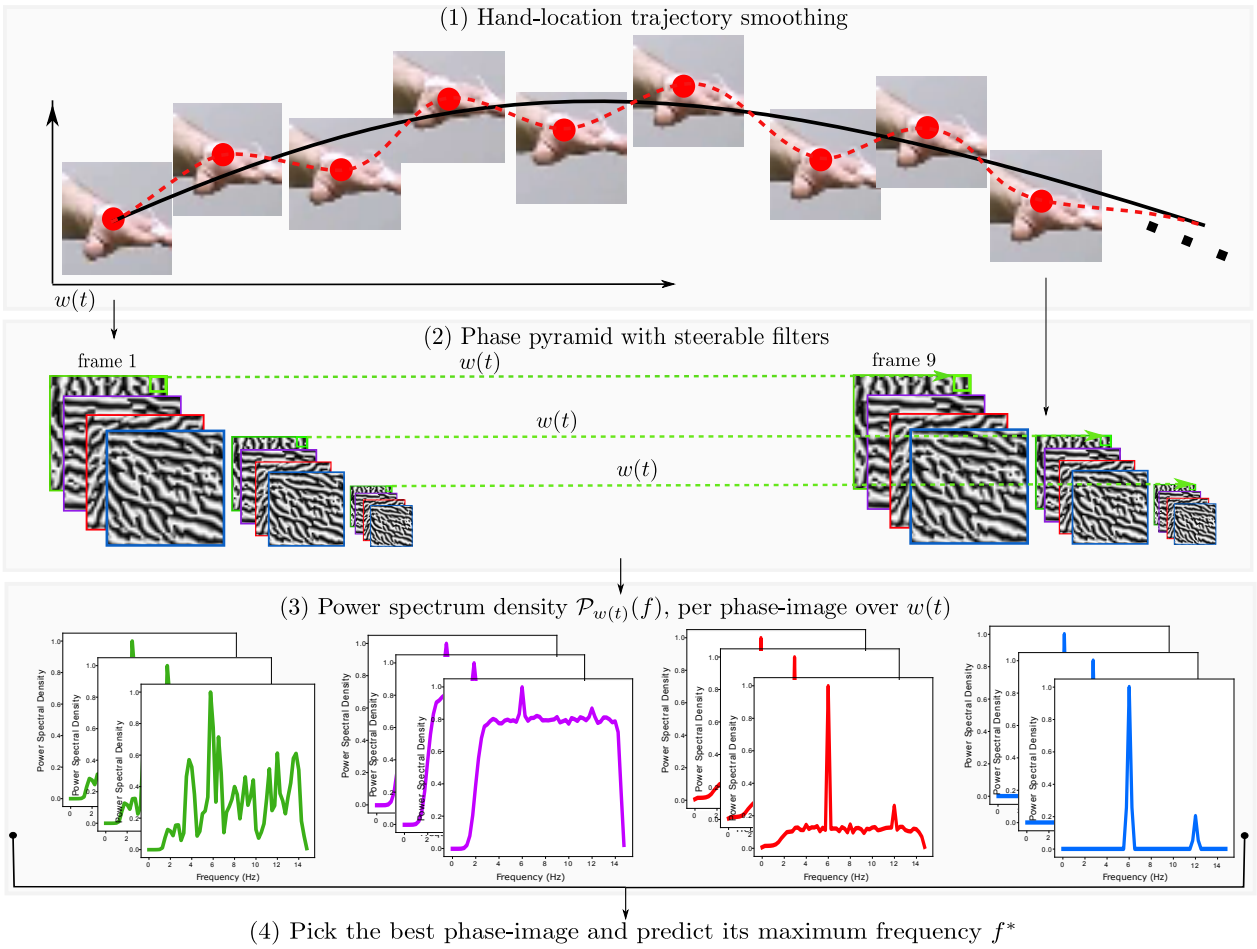

Figure 2: Eulerian hand-tremor estimation is based on frequency estimation in images. (1) The fist step is the same as in the Lagrangian illustrated in pose: detecting a Kalman-filtered smoothed hand position at every frame over a temporal window $w(t)$. (2) We crop image windows around the smoothed hand locations. Each such cropped image is transformed into a phase-pyramid with 4 orientations and 3 scales using a steerbale filter bank. (3) For every pixel, in every phase-image over the temporal window $w(t)$ we estimate a PSD (Power Sectrum Denisty). We accumulate these over the pixels in one phase-image, to obtain one PSD per phase-image. (4) We select the most informative phase-image PSD and use it to estimate the tremor-frequency.

function. We use the maximum frequency as the estimated hand-tremor frequency.

3.3. (b) Eulerian hand-tremor frequency estimation

Figure 2 illustrates the Eulerian frequency estimation. The first step is the same as in Figure 1, where the hand locations are detected using the pose estimation method in [36] and subsequently smooth the trajectory given by these hand detections using a Kalman tracker. This gives us the smooth trajectory of the hand over time, in the video. We crop image windows around the temporally smoothed locations of the hand in the video — along the black line depicted in Figure 2.(1). For each such image crop, we extract local motion information encoded as phase over different scales and orientations. Thereafter, we compute the frequency of the hand-tremor by using the most informative phase-image. Figure 2 depicts these individual steps.

3.3.1 Phase-image computation.

Works such as [10, 21, 35, 39] claim that the phase responses over time contain descriptive information regarding the motion present in the image. In [35] the use of complex steerable filters [11] is proposed for extracting local motion information. Given an input image $I(x, y)$ and a set of complex steerable filters of the form: $G^{\theta}_{\sigma} + iH^{\theta}_{\sigma}$, where $i = \sqrt{-1}$, σ defines the scale of the filter, and θ the orientation, we obtain a complex steerable pyramid by convolving

the image with this set of filters

$$(G_\sigma^\theta + iH_\sigma^\theta) \circledast I(x,y) = A_\sigma^\theta(x,y)e^{i\phi_\sigma^\theta(x,y)}, \quad (1)$$

where $\circledast$ denotes the convolution operations, and $A_\sigma^\theta(x,y)$ is the resulting amplitude for scale σ and orientation θ, and $\phi_\sigma^\theta(x,y)$ is the corresponding phase information. To obtain a phase-image, we set the amplitude to 1 and apply the inverse transformation [11] to reconstruct back the image. Examples of phase-images are depicted in Figure 2.(2). We use 4 orientations: $\theta \in \{0, \frac{\pi}{4}, \frac{\pi}{2}, \frac{3\pi}{4}\}$ and 3 scales: $\sigma \in \{1.0, 0.5, 0.25\}$, giving rise to 12 phase-images. In addition to the 12 phase-images, we add the grayscale version of the cropped hand-image. Therefore, we have in total 13 images, which we merge into a single image with 13 channels, over which we estimate the hand-tremor frequency.

3.3.2 Hand-tremor frequency estimation.

We filter each one of the 13 input channels over time with a 4^{th}-order Butterworth band-pass filter. This eliminates noisy frequencies that cannot correspond to a natural human tremor.

To reduce the effect of the considered temporal window, $w(t)$, we use an adjustable Tukey window with the parameter α set to $\frac{f_s}{N-1}$, where f_s is the sampling rate and N is the total number of frames in $w(t)$. This ensures that the video signal over time is processed in a consistent manner while allowing for adjustable temporal window sizes, $w(t)$.

Within each temporal window, $w(t)$, we estimate a PSD function, over every input channel, at every pixel location. For an input channel, c, we estimate the final PSD, $\mathcal{P}^c_{w(t)}(f)$, by averaging spatially the PSDs over the pixels in that channel. We repeat this process for all 13 channels, giving rise to 13 PSD functions.

In [4] the power spectrum is considered to be periodic at a certain frequency, f, if the PSD response at that frequency is a few standard deviations away from the mean PSD response. This is indicative of how noisy is the PSD function. We use this same criterion to pick the most informative image channel; this is the channel over which we estimate the final hand-tremor frequency. We define for each channel a score, $\mathcal{S}^c(f)$:

$$\mathcal{S}^c(f) = \sum_{w(t)} \left(\mathcal{P}^c_{w(t)}(f) - \mu_{\mathcal{P}^c_{w(t)}} - k\sigma_{\mathcal{P}^c_{w(t)}} \right), \quad (2)$$

where $\mu_{\mathcal{P}^c_{w(t)}}$ represents the mean of the PSD response, and $\sigma_{\mathcal{P}_{w(t)}}$ denotes the standard deviation, while k is an adjustable parameter. We set $k = 3$ in our experiments.

The final predicted frequency over the 13 channels becomes:

$$f^* =_f (\max_c \mathcal{S}^c(f)). \quad (3)$$

4. Experiments

We test the considered frequency estimation approaches on our tremor patient dataset, *TIM-Tremor*, containing a multitude of tasks. The anonymized *TIM-Tremor* patient data will be made publicly available.

4.1. Patient data evaluation

4.1.1 Data description.

We recorded the *TIM-Tremor* dataset, in which 55 patients are videotaped sitting in a chair and performing a multitude of tasks. The data is recorded with a Kinect^{TM} v2 device, and it consists of short HD RGB videos of resolution 1920×1080 px, and associated depth video recordings of 512×424 px using a 16-bit encoding, as well as depth videos aligned with the RGB videos following the method in [16]. The ground truth tremor frequency is measured on the wrist of the most affected hand: left/right. On this hand, during the recording, we position an accelerometer. The accelerometer recordings are included in the dataset. The hand on which the accelerometer is positioned, is annotated in the dataset for each patient. Thus, for each patient we provide a set of recorded videos of approximately 1 minute each, together with a corresponding depth-map video, an aligned depth map video, and the ground truth accelerometer recording from the most affected hand. Figure 3 displays a few examples of the recording setup together with the estimated joint locations using [36].

Data collection occurred in parallel to the standard tremor clinical evaluation. The standard tremor evaluation consists of a set of 21 tasks, which are illustrated in Figure 4.(a) and described in Figure 4.(b). The tasks vary with respect to the adopted posture: e.g. arm supported by the arm rest, or held outstretched in front of the patient, the amount of motion involved: e.g. rest – no motion, or touch-

Figure 3: Examples from the recording setup together with the predicted body joint locations using [36]. We use this to obtain the location of the hand where we estimate the tremor frequency.

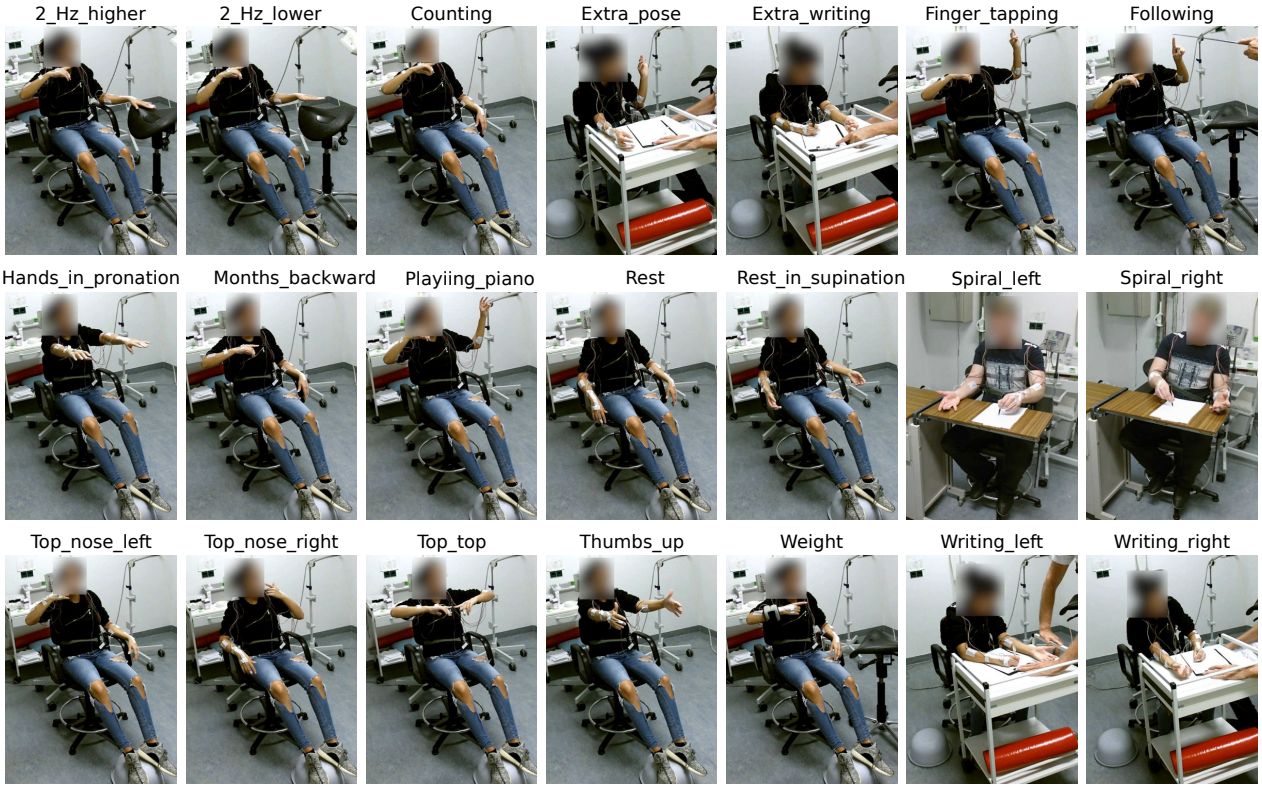

(a) Recorded tasks.

Task	Description
2_Hz_higher	Tapping in the rhythm of a flashing light, 2 Hz higher than the frequency estimated at rest.
2_Hz_lower	Tapping in the rhythm of a flashing light, 2 Hz lower than the frequency estimated at rest.
Counting	Counting backwards 100-7, with the affected arm outstretched forward.
Extra_pose	Holding a pose proposed by the medical expert to better visualize the tremor.
Extra_writing	Extra writing task with a special pen, or diverging from the standard writing task.
Finger_tapping	Tapping using the index and thumb fingers.
Following	Following a moving pointer, with the index finger of the most affected arm.
Hands_in_pronation	Hands in pronation position.
Months_backward	Naming the months backwards, with the affected arm outstretched forward.
Playing_piano	Moving the thumb across all fingers from the index to the pinky finger, and back.
Rest	Resting the arms on the chair handles.
Rest_in_supination	Resting the arms in supination position, on the chair handles.
Spiral_left	Drawing a spiral with the left hand.
Spiral_right	Drawing a spiral with the right hand.
Top_nose_left	Touching the top of the nose with the left hand.
Top_nose_right	Touching the top of the nose with the right hand.
Top_top	Holding the fingertips in front of each other, with the elbows lifted at 90 degrees angle.
Thumbs_up	Holding the thumbs up with the arms outstretched forward.
Weight	The affected arm outstretched forward, with a weight attached to the wrist.
Writing_left	Writing a given sentence with the left hand.
Writing_right	Writing a given sentence with the right hand.

(b) Explanation.

Figure 4: (a) We record motor-disorder patients in 21 tasks. Each task may elicit a tremor. (b) Short explanation of what each task involves.

ing the top of the nose – intention-oriented motion, as well as the focus of attention: e.g. distraction by mental task. Changes in tremor frequency between these tasks are analyzed by the medical expert to classify the tremor. For example, certain types of tremor are present across most or all tasks (e.g. "Parkinsonian tremor"), while other types of tremor may only occur when performing a specific task (e.g. "postural tremor" occurs only when a patient maintains a specific posture such as *Thumbs_up*), while other tremors may show considerable variation in tremor frequency between tasks (e.g. "functional tremor").

In Figure 5 we show the total number of videos recorded for each task, and the average hand tremor frequency, as estimated by the accelerometer, together with the standard deviation, computed across all 55 patients. The average tremor frequency is around 5 Hz, which is a common in tremor affections such as Parkinson and Dystonia.

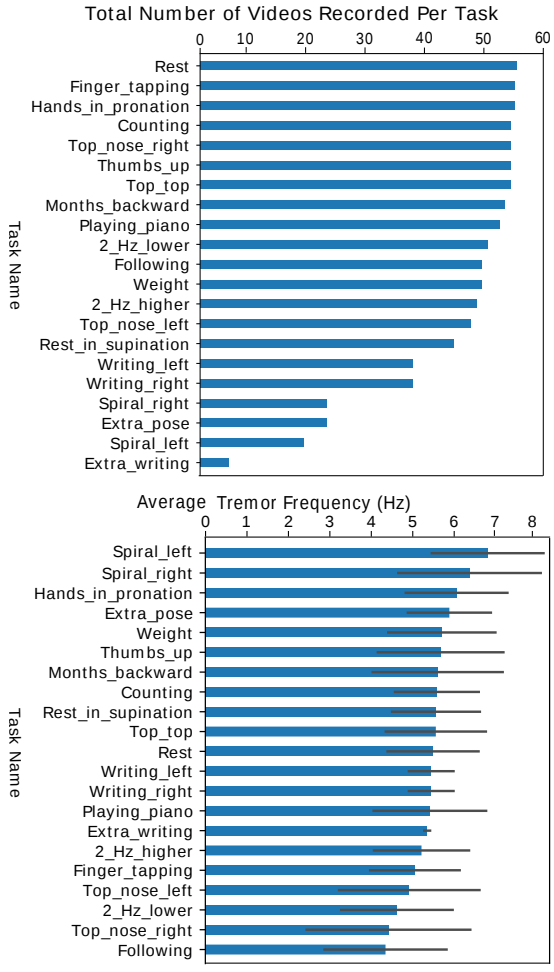

Figure 5: Top: Total number of videos recorded per task. Bottom: Average frequency and standard deviation for all tasks across all 55 patient recordings.

4.1.2 Experimental evaluation.

We estimate the body pose in the videos using the method in [36], pretrained on the MPII dataset [1]. We apply the method a every frame. We use a temporal window, $w(t)$, of 60 frames for frequency estimation. Unless stated otherwise, we evaluate our method in terms of MAE (Mean Absolute Error) with respect to the ground truth frequency detected by the accelerometer. We only evaluate on video segments in which a periodic tremor has been detected, using the accelerometer data.

4.2. Exp. 1: Design choices

In this experiment we test individual choices in the considered Lagrangian and Eulerian approaches. For the Lagrangian approach we test in **Exp 1.1** if removing the smooth trajectory, corresponding to the large motion of the hand, helps the frequency estimation. For the Eulerian approach, in **Exp 1.2** we test the added value of computing hand-tremor frequency over the phase information, rather than using only the intensity values of the image.

Exp 1.1: The need of trajectory smoothing. We experimentally compare two variants of the Lagrangian frequency estimation. The *Lag_no_smooth* variant uses raw hand trajectory points as computed by the pose estimation algorithm. The *Lag_with_smooth* variant removes the large motion of the hand obtained by subtracting the output of a Kalman tracker, which in effect retains only the small motions. The MAE numbers in Table 1 show that removing the large motion by using the Kalman tracker is beneficial to the overall performance. This is explained by the fact that subtracting the trajectory returned by the Kalman tracker from the original hand trajectory works as a data detrending step. This allows for the frequency to be estimated only over the small tremor motion. For both considered Eulerian approaches we stabilize the trajectory along which we measure the tremor by using the Kalman tracker, and subsequently perform the frequency estimation over the complete hand window.

Exp 1.2: The added value of using phase-images. In Table 2 we test the added value of using phase information for frequency estimation. We compare two variants. The *Euler_gray* variant estimates the frequency over gray-scale pixels over gray-scale hand-images, obtained by cropping the hand location along the smoothed trajectory of the hand. The *Euler_phase* variant adds the 12 phase channels as detailed in section 3.3. The phase channels allow the *Euler_phase* to more precisely capture the small motion corresponding to the tremor, because the phase is effective for describing motion. The MAE numbers in Table 2 validate that adding the phase information is beneficial for the hand-tremor frequency estimation.

Table 1: **Exp 1.1:** MAE when comparing the Lagrangian method with trajectory smoothing by using the Kalman tracker — *Lag_with_smooth*, versus not using trajectory smoothing, *Lag_no_smooth*. *Lag_with_smooth* performs slightly better than the default Lagrangian method, *Lag_no_smooth*. We highlight in bold the better performing method (lower is better).

Task	Lag_no_smooth (Hz)	Lag_with_smooth (Hz)
2_Hz_higher	1.917 (± 2.395)	**1.879** (± 2.127)
2_Hz_lower	2.248 (± 2.770)	**1.721** (± 2.266)
Counting	1.731 (± 2.336)	**1.377** (± 2.246)
Extra_pose	3.590 (± 2.369)	**1.918** (± 1.328)
Extra_writing	1.968 (± 0.000)	**1.968** (± 0.000)
Finger_tapping	1.989 (± 2.783)	**1.326** (± 1.974)
Following	1.607 (± 1.745)	**1.312** (± 1.728)
Hands_in_pronation	2.582 (± 2.154)	**2.398** (± 2.024)
Months_backward	2.544 (± 2.703)	**2.031** (± 2.500)
Playing_piano	2.443 (± 2.826)	**2.033** (± 2.516)
Rest	**3.300** (± 3.271)	3.395 (± 3.226)
Rest_in_supination	2.889 (± 3.228)	**2.059** (± 2.248)
Spiral_left	6.721 (± 1.896)	**6.721** (± 1.896)
Spiral_right	3.246 (± 1.762)	**3.148** (± 1.803)
Top_nose_left	3.743 (± 3.262)	**3.688** (± 3.242)
Top_nose_right	1.928 (± 2.323)	**1.771** (± 2.204)
Top_top	**1.388** (± 1.797)	1.669 (± 1.888)
Thumbs_up	1.694 (± 1.807)	**1.694** (± 1.836)
Weight	**2.660** (± 2.667)	2.795 (± 2.569)
Writing_left	2.557 (± 1.139)	**2.557** (± 1.139)
Writing_right	2.557 (± 1.139)	**2.557** (± 1.139)
Average MAE	2.633 (± 2.208)	**2.382** (± 1.995)

Table 2: **Exp 1.2:** MAE showing the added value of the phase information. We compare the *Euler_gray* — Eulerian frequency estimation over grayscale hand-images, with *Euler_phase* – Eulerian frequency estimation over 12 phase-images and 1 grayscale image. Adding the 12 extra phase-images is beneficial for the frequency estimation. We highlight in bold the better performing method (lower is better).

Task	Euler_gray (Hz)	Euler_phase (Hz)
2_Hz_higher	0.882 (± 1.142)	**0.857** (± 1.533)
2_Hz_lower	1.335 (± 2.022)	**0.984** (± 1.333)
Counting	0.767 (± 1.252)	**0.472** (± 0.780)
Extra_pose	**1.180** (± 2.006)	1.623 (± 1.185)
Extra_writing	0.984 (± 0.000)	**0.984** (± 0.000)
Finger_tapping	0.492 (± 0.893)	**0.385** (± 0.647)
Following	0.820 (± 1.327)	**0.557** (± 0.503)
Hands_in_pronation	1.271 (± 1.755)	**1.066** (± 1.506)
Months_backward	**1.133** (± 1.848)	1.219 (± 1.933)
Playing_piano	1.148 (± 1.832)	**1.148** (± 1.714)
Rest	1.459 (± 1.759)	**1.253** (± 1.770)
Rest_in_supination	**1.475** (± 1.919)	1.537 (± 1.728)
Spiral_left	3.278 (± 1.671)	**2.951** (± 1.391)
Spiral_right	3.246 (± 2.936)	**2.509** (± 2.021)
Top_nose_left	2.595 (± 2.216)	**1.776** (± 2.008)
Top_nose_right	3.108 (± 2.739)	**2.164** (± 2.015)
Top_top	0.860 (± 1.311)	**0.720** (± 1.200)
Thumbs_up	1.002 (± 1.419)	**1.002** (± 1.273)
Weight	1.207 (± 1.695)	**0.961** (± 1.226)
Writing_left	**0.394** (± 0.573)	0.492 (± 0.538)
Writing_right	**0.394** (± 0.573)	0.492 (± 0.538)
Average MAE	1.382 (± 1.566)	**1.198** (± 1.278)

4.3. Exp 2: Eulerian versus Lagrangian tremor frequency estimation

In Figure 6 we display the accuracy of our proposed frequency estimation methods over the complete set of 55 patient recordings, for all tasks. We show in dotted blue line the number of videos per task where a periodic tremor was detected, according to the accelerometer data. In corresponding color, we show the number of videos in which we have correctly estimated the hand-tremor frequency, for each frequency estimation method: *Euler_phase* is the Eulerian method using 12 phase-channels and 1 grayscale channel; *Euler_gray* is the Eulerian method on image intensity information only; *Lag_no_smooth* is the Lagrangian method without Kalman trajectory smoothing; *Lag_with_smooth* is the Lagrangian method with Kalman trajectory smoothing. We consider an estimated tremor frequency to be correct if the MAE between the accelerometer frequency and the one estimated by the method is lower than 1 Hz.

Figure 6 shows that on average the Eulerian frequency estimation methods are more precise than the Lagrangian methods. The gain of using the Eulerian approaches is especially clear for the *Weight* task and the *Hands_in_pronation* task. Figure 7 displays the MAE scores per patient for these two tasks. To avoid over-cluttering the image, we only show the best Lagrangian method: *Lag_with_smooth*, Lagrangian with Kalman trajectory smoothing, and the best Eulerian method: *Euler_phase*, Eulerian over 12 phase channels and 1 grayscale channel. The Eulerian method gives more precise frequency estimates for some of the patient recordings, while for others it performs similar to the Lagrangian method. The tasks are not characterized by large hand motion. The gain of the Eulerian method over the Lagrangian is explained by the Eulerian method better describing the subtle changes in image information over time at the hand location. Therefore, the Eulerian method more accurately captures the tremor in tasks that do not involve large hand motion, but exhibit small motion.

4.4. Limitations

From the comparison of results, we show the superiority of the *Eulerian-based* methods in tremor frequency analysis and also prove the effectiveness of using phase information

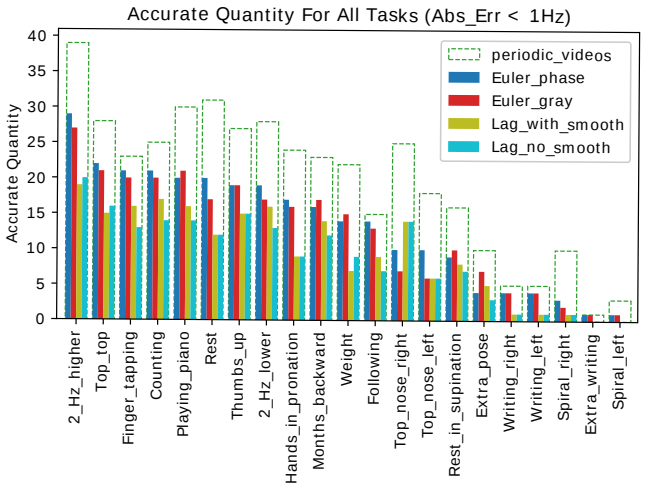

Figure 6: **Exp 2:** We report accuracy on all recorded tasks, over the 55 patient recordings (higher is better). We consider the hand-tremor frequency to be correctly estimated for a task if the MAE (Mean Absolute Error) for that task is lower than 1 Hz. We plot in dotted blue line the total number of videos recorded for each task, on which we have detected a periodic tremor. For each of our considered methods we show the number of videos for which the frequency was correctly estimated. On average the Eulerian methods perform better than the Lagrangian methods.

and trajectory smoothing. However, this research is still far away for real application purpose compared to traditional clinical approaches. The biggest challenge comes from the complexity of the real situation which limits to get a perfect estimation accuracy. On the one hand, a basic assumption for our *Eulerian-based* methods is the hand shape does not change overtime, which is not satisfied some tasks such as *Playing_piano* and *Extra_pose*; on the other hand, for tasks with a big movement, we still can not get a high estimation accuracy even with the help of trajectory smoothing effect. The later problem is caused by the erratic of changing hand background, but it can be solved if recording new videos under a pure white background. Another limitation comes from the poor performance of human pose estimation module in specific situations like a big area of body occlusion by a table or self-occlusion caused by bad filming angle. These occlusions will cause a decline in the accuracy of hand position prediction, thus lead to an inaccuracy of frequency estimation, especially for the *Lagrangian* methods which totally depend on the trajectory points.

5. Conclusions and Future work

We consider the task of hand-tremor frequency estimation from RGB videos. We propose two different approaches for measuring human hand-tremor frequencies:

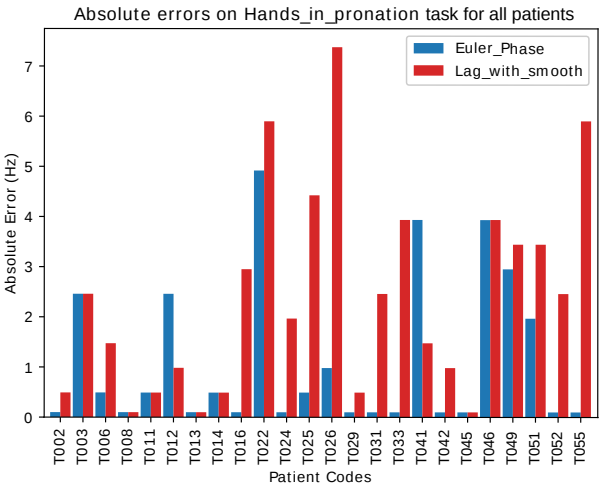

(a) *Hands_in_prontation* task.

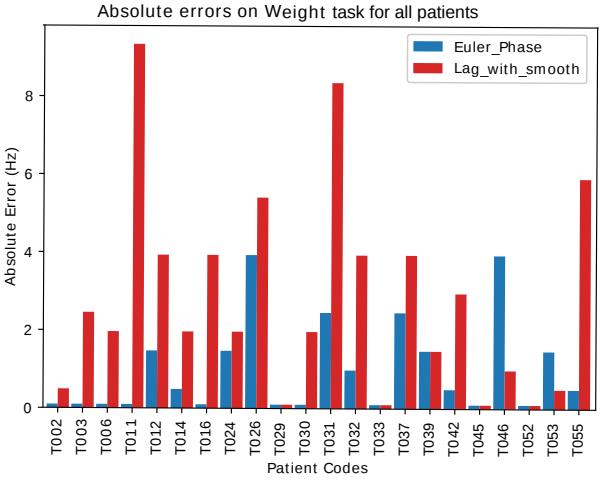

(b) *Weight* task.

Figure 7: **Exp 2:** The MAE per patient, for the two tasks where the Eulerian methods performed better than the Lagrangian methods (lower is better). To avoid overcluttering the image, we plot only the best performing Lagrangian method: *Lag_with_smooth* — Lagrangian method with Kalman trajectory smoothing, and the best performing Eulerian method: *Euler_phase* — Eulerian method using 12 phase channels and 1 grayscale channel. The Lagrangian method makes large frequency estimation mistakes on a few patient videos, while the Eulerian method is more precise on some of the patient videos. Note: for certain patients the task has not been recorded or no stable frequency, according to the accelerometer, has been found.

(a) Lagrangian hand-tremor frequency estimation, using the trajectory of the hand motion in the image plane throughout the video, to assess the hand-tremor frequency; and (b) Eulerian hand-tremor frequency estimation, which measures the change in the image information over time, at the loca-

tion of hand in the image plane. We experimentally evaluate two variants of each approach on the *TIM-Tremor* dataset containing 55 patient recordings performing a multitude of tasks. The video recordings, together with the associated ground truth accelerometer recordings, and aligned depth maps, will be made publicly available. From our experimental analysis we learned that the Eulerian approaches are more accurate on average than the Lagrangian methods, with the difference being substantial on tasks on which there is a limited amount of large hand motion, but where there is a small hand-tremor motion present.

To further improve the estimation performance, we still have many techniques to try in different parts. First of all, we can take the benefits from other the-state-of-art human pose estimation approaches, such as the work in [20] which incorporates human parsing information to adapt the pose estimation model, to increase the hand position prediction accuracy. This will take a promotion for all proposed methods but needs much time to train the deep learning model. Another possible modification is about the trajectory smoothing method. The kalman filter is the optimal linear filter only when we can perfectly describe the physical model for the hand motion. So we believe other adaptable filter algorithms like the particle filter will upgrade the smoothing performance.

References

[1] M. Andriluka, L. Pishchulin, P. Gehler, and B. Schiele. 2d human pose estimation: New benchmark and state of the art analysis. In *CVPR*, pages 3686–3693, 2014.

[2] A. Bulat and G. Tzimiropoulos. Human pose estimation via convolutional part heatmap regression. In *ECCV*, pages 717–732. Springer, 2016.

[3] J. Carreira, P. Agrawal, K. Fragkiadaki, and J. Malik. Human pose estimation with iterative error feedback. In *CVPR*, pages 4733–4742, 2016.

[4] R. Cutler and L. S. Davis. Robust real-time periodic motion detection, analysis, and applications. *PAMI*, 22(8):781–796, 2000.

[5] H. Dai, P. Zhang, and T. C. Lueth. Quantitative assessment of parkinsonian tremor based on an inertial measurement unit. *Sensors*, 15(10):25055–25071, 2015.

[6] A. Davis, K. L. Bouman, J. G. Chen, M. Rubinstein, F. Durand, and W. T. Freeman. Visual vibrometry: Estimating material properties from small motion in video. In *CVPR*, pages 5335–5343, 2015.

[7] L. di Biase, J. S. Brittain, S. A. Shah, D. J. Pedrosa, H. Cagnan, A. Mathy, C. C. Chen, J. F. Martín-Rodríguez, P. Mir, L. Timmerman, et al. Tremor stability index: a new tool for differential diagnosis in tremor syndromes. *Brain*, page awx104, 2017.

[8] R. J. Elble and J. McNames. Using portable transducers to measure tremor severity. *Tremor and Other Hyperkinetic Movements*, 6, 2016.

[9] M. Elgharib, M. Hefeeda, F. Durand, and W. T. Freeman. Video magnification in presence of large motions. In *CVPR*, pages 4119–4127, 2015.

[10] D. J. Fleet and A. D. Jepson. Computation of component image velocity from local phase information. *IJCV*, 5(1):77–104, 1990.

[11] W. T. Freeman, E. H. Adelson, et al. The design and use of steerable filters. *TPAMI*, 13(9):891–906, 1991.

[12] R. Goldenberg, R. Kimmel, E. Rivlin, and M. Rudzsky. Behavior classification by eigendecomposition of periodic motions. *Pattern Recognition*, 38(7):1033–1043, 2005.

[13] M. D. Hssayeni, M. A. Burack, and B. Ghoraani. Automatic assessment of medication states of patients with parkinson's disease using wearable sensors. In *EMBC*, pages 6082–6085. IEEE, 2016.

[14] H. Jeon, W. Lee, H. Park, H. J. Lee, S. K. Kim, H. B. Kim, B. Jeon, and K. S. Park. Automatic classification of tremor severity in parkinsons disease using a wearable device. *Sensors*, 17(9):2067, 2017.

[15] H. Kayaba and Y. Kokumai. Non-contact full field vibration measurement based on phase-shifting. In *CVPR*, pages 3655–3663, 2017.

[16] J. Kooij. Sensecap: synchronized data collection with microsoft kinect2 and leapmotion. In *ACMMM*, pages 1218–1221. ACM, 2016.

[17] J. Kooij and J. van Gemert. Depth-aware motion magnification. In *European Conference on Computer Vision*, pages 467–482. Springer, 2016.

[18] O. Levy and L. Wolf. Live repetition counting. In *CVPR*, pages 3020–3028, 2015.

[19] C. Lu and N. J. Ferrier. Repetitive motion analysis: Segmentation and event classification. *PAMI*, 26(2):258–263, 2004.

[20] X. Nie, J. Feng, Y. Zuo, and S. Yan. Human pose estimation with parsing induced learner. In *Proceedings of the IEEE Conference on Computer Vision and Pattern Recognition*, pages 2100–2108, 2018.

[21] S. L. Pintea and J. C. van Gemert. Making a case for learning motion representations with phase. In *ECCV workshop*, pages 55–64, 2016.

[22] L. Pishchulin, E. Insafutdinov, S. Tang, B. Andres, M. Andriluka, P. V. Gehler, and B. Schiele. Deepcut: Joint subset partition and labeling for multi person pose estimation. In *CVPR*, pages 4929–4937, 2016.

[23] R. Polana and R. C. Nelson. Detection and recognition of periodic, nonrigid motion. *IJCV*, 23(3):261–282, 1997.

[24] V. Ramakrishna, D. Munoz, M. Hebert, A. J. Bagnell, and Y. Sheikh. Pose machines: Articulated pose estimation via inference machines. In *ECCV*, 2014.

[25] Y. Ran, I. Weiss, Q. Zheng, and L. S. Davis. Pedestrian detection via periodic motion analysis. *IJCV*, 71(2):143–160, 2007.

[26] Z. M. Ripin and P. Y. Chan. Pathological hand tremor measurementchallenges and advances. In *ICIBELS*, pages 3–8, 2017.

[27] K. Roy, G. S. Rao, and S. M. Anouncia. A learning based approach for tremor detection from videos. In *ICOS*, pages 71–76. IEEE, 2013.

[28] T. F. Runia, C. G. Snoek, and A. W. Smeulders. Real-world repetition estimation by div, grad and curl. In *CVPR*, pages 9009–9017, 2018.

[29] B. Soran, J. Hwang, S. Lee, and L. Shapiro. Tremor detection using motion filtering and svm. In *ICPR*, pages 178–181, 2012.

[30] C. J. Tralie and J. A. Perea. (quasi) periodicity quantification in video data, using topology. *CoRR*, 2017.

[31] Z. Uhríková, E. Růžička, V. Hlaváč, and C. D. Nugent. Treman: a tool for measuring tremor frequency from video sequences. *Movement Disorders*, 25(4):504–506, 2010.

[32] Z. Uhríková, O. Šprdlík, M. Hoskovcová, A. Komárek, O. Ulmanová, V. Hlaváč, C. D. Nugent, and E. Růžička. Validation of a new tool for automatic assessment of tremor frequency from video recordings. *Journal of neuroscience methods*, 198(1):110–113, 2011.

[33] B. Victor, Z. He, S. Morgan, and D. Miniutti. Continuous video to simple signals for swimming stroke detection with convolutional neural networks. *CVPR*, 2017.

[34] M. Vidailhet, E. Roze, and H. A. Jinnah. A simple way to distinguish essential tremor from tremulous parkinsons disease. *Brain*, 140(7):1820–1822, 2017.

[35] N. Wadhwa, M. Rubinstein, F. Durand, and W. T. Freeman. Phase-based video motion processing. *SIGRAPH*, 32(4):80, 2013.

[36] S. Wei, V. Ramakrishna, T. Kanade, and Y. Sheikh. Convolutional pose machines. In *CVPR*, pages 4724–4732, 2016.

[37] L. Xia, B. Zou, H. Liu, H. Su, and H. Qianghui. A new method for evaluating postural hand tremor based on cmos camera. *Optik-International Journal for Light and Electron Optics*, 126(5):507–512, 2015.

[38] P. Zarchan and H. Musoff. Fundamentals of kalman filtering: A practical approach, 2013.

[39] Y. Zhang, S. L. Pintea, and J. C. van Gemert. Video acceleration magnification. *CVPR*, 2017.

2

SUPPLEMENTAL MATERIAL

CONTENTS

1

INTRODUCTION

1.1. PROBLEM STATEMENT

A tremor is a kind of involuntary rhythmic movement which can be related to one or more body parts of a person [1]. Tremors mostly occur in the hands of a human body. The hand tremors also characterize a lot of neurodegenerative diseases like Parkinson disease. They may significantly affect the patients in daily life and work. To accurately diagnose the condition of a patient and initiate the most appropriate treatment, it is necessary to make computerized tremor analysis. Two of the essential characteristics of tremor assessed by tremor analysis are frequency and amplitude [2]. In this research, we only focus on the frequency characteristic of tremors.

In most conventional methods of tremor analysis, some sensor devices, such as accelerometers, are located on a specific part of patients to record tremor activity. Another widely used method is Electromyography (EMG) [3] which can generate an electromyogram with valuable frequency information by recording the electrical activity of skeletal muscles. Since tremors are quasi-sinusoidal movements [2], it is feasible to obtain the frequency information by analyzing the power spectral density of the tremor signal.

Those old methods are proved to be useful and reliable in many clinical and biomedical applications, but their disadvantages are also apparent. The inevitable trouble is that all of them need a special-purpose medical hardware for collecting the tremor signal and the devices must touch the skin of a patient. For EMG method, it even requires skin preparation and insertion of the needle electrode. Apart from the inconvenience, complex operating procedures can cause possible operational errors. In our research, we propose a novel method to detect the tremor frequency using only an ordinary RGB camera.

1.2. CHALLENGES AND PROPOSED METHOD

POSE ESTIMATION

In our proposed method, given a video which records the movement of the hands of a patient, the first step is to find the hand joint position in a video accurately. To collect the video data set, a common camera is stationary and placed at an appropriate distance from the patient. A patient needs to finish various kinds of tasks following the instruction of a doctor. The diversity of poses of a patient makes the location step on the target joint much harder, cause the hand shape changes while doing some tasks such as imitating the action of playing the piano and tapping using the index and thumb finger. So it is a bad idea if we use a tracking strategy to locate the hand position in a video even with a state-of-the-art tracking algorithm, because most object tracking techniques can only output rough positions of the object among frames, and object shape change increases the possibility of missing tracking target.

We propose to implement a human pose estimation strategy to extract the hand locations in a video. Human pose estimation has been a favorite research topic for a long time, and its target is to detect and estimate the configuration of the articulation structure of a person [4]. With the advantage of human pose estimation, we can always locate the positions of hands without the adverse effect of changing hand shape. Since 2014, many methods based on convolutional neural networks (CNN) are proved to be effective and achieve astonishing results [5–8]. We opt for the Convolutional Pose Machine (CPM) in [8] because of its ease of usage and robustness.

SUBTLE MOTION

Although we only focus on the frequency characteristic of tremors in this research task, it can be complicated to make frequency analysis if the tremor is not well captured in a video when the camera is too far way to a patient. The reality that the orientation of hand tremors varies among different patients and different tasks also increases the difficulty in achieving a good frequency estimation accuracy. In [9, 10], it has been proved that most naked eyes invisible tremors can be magnified through a complex steerable pyramid. We leveraged the effectiveness and robustness in subtle multidirectional motion representation of a complex steerable pyramid to tackle with the above challenges.

In more realistic case, the subtle motions of hand tremor are combined with a large motion in specific tasks, such as raising an arm then touching the top of the nose with a hand from a far end of the body. We implemented two approaches based on motion descriptions in two distinct coordinate systems to compare their applicability for our purpose. The two coordinate systems are Lagrangian coordinate system and Eulerian coordinate system respectively. We proved the superiority of the latter than the former through complete experiments in our case.

FREQUENCY ESTIMATION

For frequency estimation, we first need to make an underlying assumption that the value change of a kind of representations in each pixel position is an indicator of the tremor frequency. The representations may be in a domain of grayscale, RGB, light flow, phase or any other. Here we use phase images since the usage of the complex steerable pyramid.

There is much redundant information for frequency estimation in a video as we are only interested in the frequency characteristic of hand tremor. For this reason, we crop a fixed size box area centered on the wrist based on the results of the pose estimations in all frames. In a frame sequence, the fluctuating values form an intensity series in each pixel position, and it can be considered as a sampling of a time domain signal. After preprocessing, we convert the time signal sampling to a frequency domain signal by Fast Fourier transform. We select the most dominant frequency component in the power spectral density as the result of frequency estimation.

1.3. OUTLINE

The rest of this report is structured as follows. First, we present the needed preliminary and detailed methodology in Section 2 for quickly understanding the work presented in the scientific paper. It covers an extensive introduction about *Human pose estimation*, *Trajectory smoothing*, and *Phase-based method*. In Section 3 we first give the details about the benchmark, including the raw data and the way to estimate frequency from accelerometer data. Then we discuss the parameter selection of experiments and finally present frequency estimation results of all tasks in our dataset with a short conclusion.

2

PRELIMINARY

This chapter describes the needed preliminary and detailed methodology for easily understanding the work presented in the scientific paper. It starts with an introduction to the idea of human pose estimation. It covers the basics of *Pose Machines* and *Convolutional Pose Machines* for understanding the first step in hand-tremor frequency estimation. Then it is followed by introducing the methods for trajectory smoothing, in which also gives an introduction of two coordinate systems for motion representation and how to use the *Kalman filters* for smoothing. In the last part, we talk about the proposed phase-based method by employing the *Complex Steerable Pyramid*.

2.1. HUMAN POSE ESTIMATION

Human pose estimation is the first step in the project, the goal of this module is to estimate the location of the affected hand. We opt for the Convolutional Pose Machines (CPMs) in [8] because of its ease of usage and robustness.

2.1.1. POSE MACHINES

The *pose machine* is a modular model built on the architecture of inference machine for articulated human pose estimation[11]. To be more detailed, the pose machine can estimate the locations of 14 body joints in a picture, including head, neck, shoulders, elbows, wrists, hips, knees and ankles.

The pose machine improves the estimation accuracy by making full use of spatial relevance among different body parts and joint feature information in multiple scales [11]. The structure of the pose machines is shown in Figure 2.1. In every stage, a predictor g_i is trained to generate belief maps b_i for all concerned joints, which indicate the possibilities of joint locations in an image.

At the beginning, a feature extractor h_1 produces feature maps x from the input image then passes x to the first predictor to generate b_1. Then in the subsequent stages where $i > 1$, to exploit spatial correlation on the joints of the entire body, the pose machines apply a context feature function ψ to refine the confidence map b_{i-1} into the context features ψ_i. The predictors g_i generate new belief maps b_i based on context features ψ_i and new feature maps x'. The image patch area for generating feature maps x' increases in each stage to obtain joint information in multiple scales.

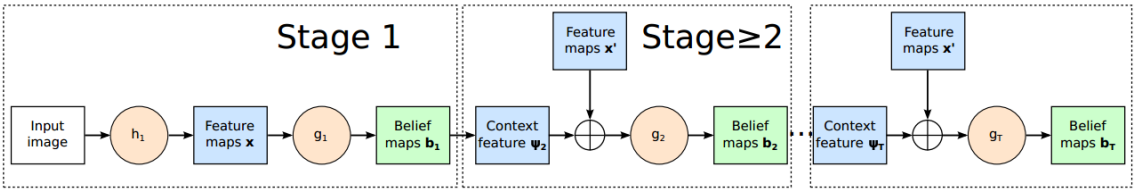

Figure 2.1: **The structure of the pose machines [12]:** The pose machines contain consecutive stages. In each stage, the belief maps b_i are passed to the next stage for refinement. From the second stage until the last stage, the spatial relevance between multiple body parts and target feature information in multiple scales are incorporated and exploited.

2.1.2. CONVOLUTIONAL POSE MACHINES

The convolutional pose machines (CPMs) incorporate the convolutional neural network (ConvNet) into the framework of the pose machines [8]. ConvNet has been proved its superpower in many applications of analyzing visual imagery, especially for its excellent ability to learn features for both image and spatial context directly from data. With the advantages provided by ConvNet, CPMs achieved outstanding performance on some standard benchmarks.

As depicted in Figure 2.2, the CPMs replace the feature computation module in each stage of the pose machines with ConvNet. In stage 1, CPMs predicts part beliefs from only local image evidence. The evidence is *local* because the related field for the deep network in the first stage is constrained to a small patch around the output pixel location. The feature extractor h_i in each stage is composed by 4 convolutional layers with 3 pooling layers. The predict function of g_i in the pose machines is substituted by a classifier consists of one 9×9 and two 1×1 convolutional layers. Moreover, to address vanishing gradients problem, a L_2 loss function f_i is added at the end of the stage for providing local supervision during training. The structure in stage 2 repeats for all subsequent stages. The same as the pose machines, the predictor in succeeding stages generates new belief maps based on new joint features and the additional information from the previous stage, and delivers new belief maps to the next stage for further refinement.

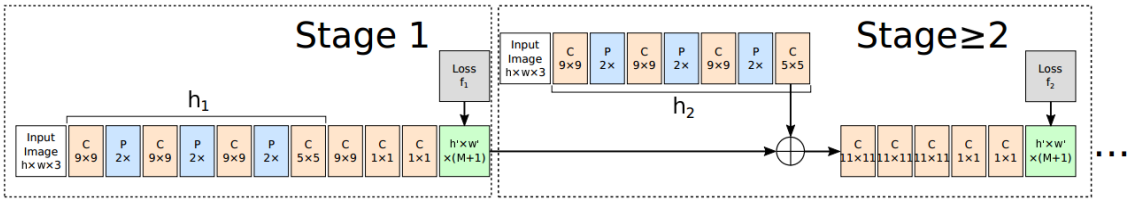

Figure 2.2: **Structure of the CPM [12]:** The insets for each stage correspond to the ones in Figure 2.1 one by one. While the ConvNet equips the CPMs a better ability to extract feature information. *C* and *P* in the illustration represent Pooling layer and Convolution layer respectively.

2.2. TRAJECTORY SMOOTHING

We start by human pose estimation, and this module gives an estimation of the affected hand location in every frame. The quantitative analysis of CPMs in [8] shows a high detection rate on the *MPII Human Pose Dataset*[5] and the *Extended Leeds Sports Dataset*[13]. The results show that the percentage correctness keypoint(PCK) of CPMs can exceed 90% in some cases with a 0.2 normalized distance. Although the performance of CPMs is relatively excellent, there is always inevitable error in the position estimation compared to manual hand annotation. The case of error is shown in figure 2.3. This hand position estimation error may introduce unacceptable error for all proposed methods in frequency estimation.

(a) Frame i (b) Frame i+1

Figure 2.3: **Error in CPM output:** There is a part of two consecutive frames, and the dot positions are the estimated hand locations from CPMs which are slightly different, ideally should be at the same position on hand surface. The big square area is cropped for the next step of frequency estimation. The small square area stands for a fixed pixel position relative to the dot center. It indicates a small error in the estimated hand location will lead to a shift for all pixel positions in the box area. It will result in an unacceptable error in the step of frequency estimation.

In addition to the non-accurate hand position estimation, large motions when executing a specific task also bring a challenge to detect a periodic signal. Figure 2.4 shows a large motion leads to a situation in which

the background in the cropped frames changes irregularly, from cables to patient's t-shirt. These random changing values in the background are low-frequency noise compared to the hand tremor signal we desired. What is worse is that the hand area only accounts for a small part of the box area size, so that the noise will be overwhelming to the real dominant frequency component.

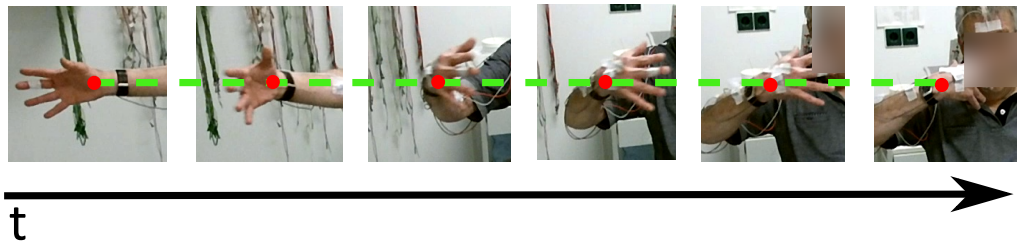

Figure 2.4: **Changing background in large motion:** The screen captures describe a situation in which a large motion leads to an irregular change for each background pixel position in the cropped frames. The red dots positions are the estimated hand locations from CPM which are slightly different.The green dash line indicates the hand position is always in the center of the box area. The messy background noise will bury out the tremor signal.

we propose a trajectory smoothing strategy to tackle the problems caused by inevitable errors in hand position estimation and large motions. With the help of smoothing, not only the errors in hand position estimation can be removed as process noise, but the background change will also stabilize. We implement a smoothing method using the Kalman filter under two different coordinate systems and compare their applicability for our purpose. The background for the two coordinate systems and the principle of smoothing the trajectory using the Kalman filter will be introduced in the next two subsections.

2.2.1. TWO COORDINATE SYSTEMS

There are two main standards for a motion description: the *Lagrangian coordinate system* where the viewer tracks an individual target as its position changes in the space-time, and the *Eulerian coordinate system*, which is a way of following a mobile target but also keep an eye on another moving reference overtime. In general, the reference in the two coordinates to describe the motion of the object are different. For example, if we are going to describe the movement of a pendulum in a moving clock, the reference object is the earth ground in Lagrangian, while in Eulerian it is the clock itself.

LAGRANGIAN COORDINATE SYSTEM

In the Lagrangian coordinate system, the target hand is tracked over time, and we only take the hand positions into account instead of the value changes in some pixel positions among a sequence of frames. Figure 2.5 indicates the representation of hand positions in the Lagrangian coordinate system. The real hand tremor signal is obtained by subtracting the large motion positions from the estimated hand positions.

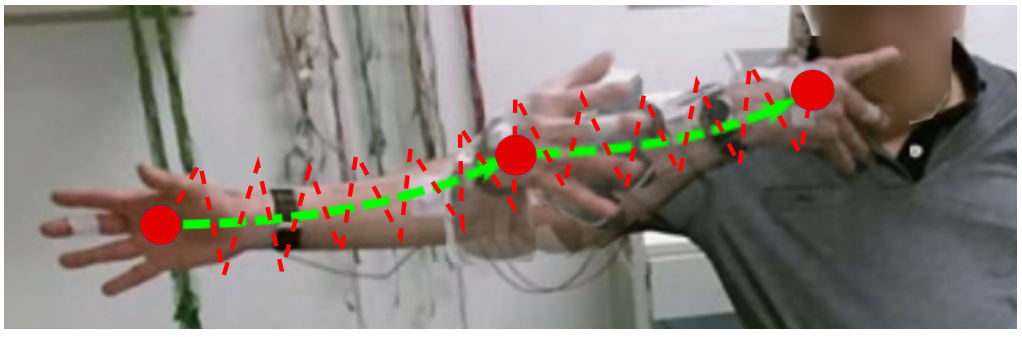

Figure 2.5: **Hand positions in Lagrangian:** The red dots are the estimated hand positions. The hand motion is characterized by a large motion, depicted by the green dash line, and a tremor in the approximately vertical direction, depicted by the red dotted line. We get the real hand tremor signal by subtracting the large motion positions from the estimated hand positions in Lagrangian coordinate system.

EULERIAN COORDINATE SYSTEM

In the Eulerian coordinate system, we also need to track the target hand in every frame, but we will crop the target hand area per frame and integrate the frequency-domain signals at all pixel positions into a one-

dimensional signal. Figure 2.6 depicts that the smoothing trajectory determines the box positions among the whole frames of a video, then we only focus on the position changes in the cropped box. Since our Eulerian motion representation approach with a smoother can be adopted under the big movement situation, it is superior to the traditional Eulerian method in which the box area is usually initialized at the first frame and kept staying at the same location in a video.

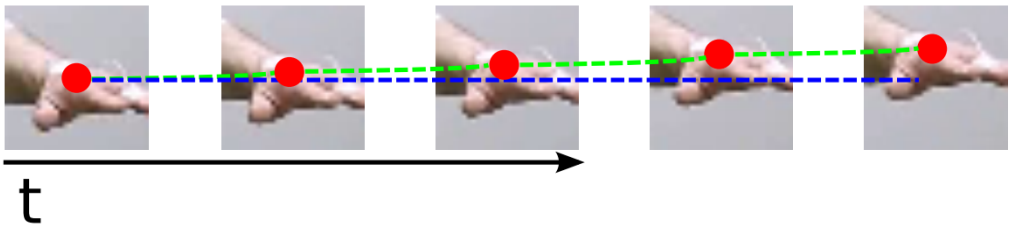

Figure 2.6: **Hand positions in Eulerian[12]:** The red dots are the estimated hand positions, and the green dash line connects the center of the target hand. The box location is stabilized by the smoothing trajectory, depicted by the blue dash line. It indicates the Eulerian coordinate observes the relative movement of the target hand by taking the center of the box as a reference.

2.2.2. THE KALMAN FILTER

The Kalman filter is an optimal recursive data processing algorithm. In recent years, it has also been applied in many research fields of computer vision, such as face recognition, image segmentation, image edge detection, and so on[14]. The Kalman filter has many derivatives under different circumstances, for example, *The Extended Kalman Filter (EKF)* applied in a process to be estimated is non-linear. In this section, we will only talk about *The Linear Kalman Filter* for the linear stochastic process and study how to use it for hand movement trajectory smoothing.

THE BASIS OF THE LINEAR KALMAN FILTER

The linear Kalman filter can have optimal solutions only in linear cases and when all noise are Gaussian[15]. In a random process, we usually have two kinds of noise, the process noise which indicates the uncertainty between the reality and process model, and the measurement noise which represents noise characteristics of the sensor's measurement capability.

The linear Kalman filter estimates the state of a linear system at a time *t* from a prior time *t-1* according to the equation:

$$x_t = A_t x_{t-1} + B_t \mu_t + \omega_t \tag{2.1}$$

where

- x_t is the state vector containing state features like position and velocity of the system at time t
- A_t is state transition matrix which describes the influence of state x_{t-1} to state x_t (e.g., the position and velocity at time $t-1$ both affect the position at time t)
- μ_t is control vector containing all control inputs (e.g., the gravity acceleration on a free-falling ball)
- B_t is control input matrix which is used to define linear equations for any control factors in μ_t
- ω_t is the vector containing process noise terms. They are assumed to be independent, white, and with normal probability distributions, i.e., $p(\omega_t) = N(0, Q_t)$

State measurements of the system can also be described, according to the model:

$$z_t = H_t x_t + v_t \tag{2.2}$$

where

- z_t is the vector of measurements
- H_t is the transformation matrix that maps the state vector terms into the measurement vector
- v_t is the vector containing measurement noise terms. It has same characteristics as process noise ω_t except its normal distribution covariance matrix is given by R_t, i.e., $p(v_t) = N(0, R_t)$

In practice, Q_t and R_t might vary with each time step and measurement, but they are used to be considered as constant.

The Kalman filter algorithm maily takes two stages: *prediction* and *update*, then it yields the best estimate $\hat{x}_t$ regarding sum-of-squares error through an iterative feedback loop with above two steps. In the *prediction stage*, the mean and covariance of the current state are estimated with two equations:

$$\hat{x}_{t|t-1} = A_t \hat{x}_{t-1|t-1} + B_t \mu_t \tag{2.3}$$

$$P_{t|t-1} = A_t P_{t-1|t-1} A_t^T + Q_t \tag{2.4}$$

where P_t is the covariance matrix, of which the terms of main diagonal and off-diagonal are respectively the variances and covariances associated with the corresponding terms in the state vector. Equation 2.3 is called state prediction which describes the probability from this state to next state, and equation 2.4 is called covariance prediction which predicts how much process error in current time step.

The *update stage* equations are given by:

$$\hat{x}_{t|t} = \hat{x}_{t|t-1} + K_t(z_t - H_t \hat{x}_{t|t-1}) \tag{2.5}$$

$$P_{t|t} = P_{t|t-1} + K_t H_t P_{t|t-1} \tag{2.6}$$

$$K_t = P_{t|t-1} H_t^T (H_t P_{t|t-1} H_t^T + R_t)^{-1} \tag{2.7}$$

where K_t is called the *Kalman gain* to moderate the prediction, H_t is the observation matrix. A state vector multiply by H_t will be translated to a measurement vector. Equation 2.5 gives an estimate of new state and equation 2.6 updates the new estimate of overall error.

As a summary of Equations (2.3) to (2.7), we give the Flowchart 2.7 to show how the Kalman filter works.

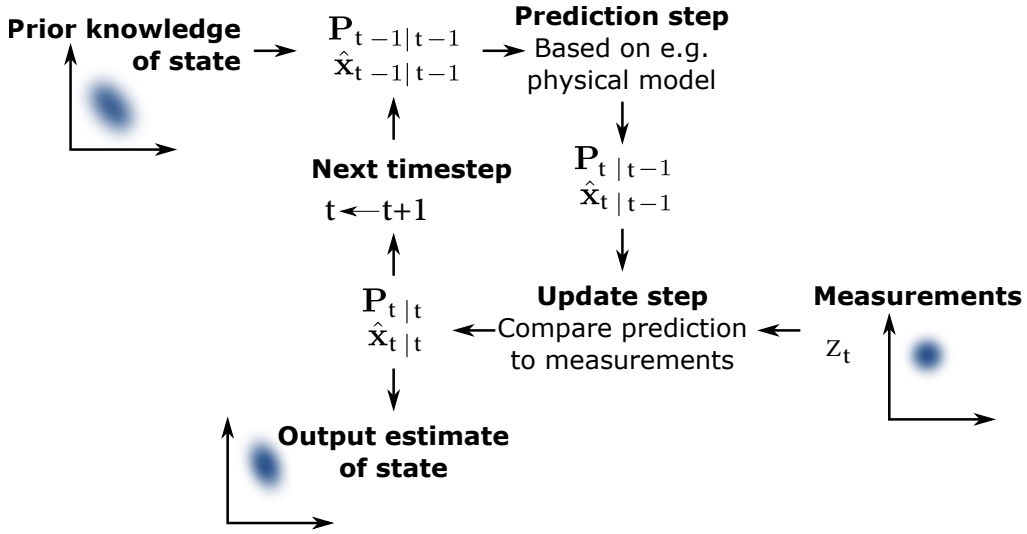

Figure 2.7: **How the Kalman filter works [15]:** The Kalman filter keeps predicting the state of the system and returns uncertainty of the estimate based on the transition model and new measurements. The blue area represents a distribution probability of a process state in 2D dimension. Through an iterative feedback loop with two steps: *Prediction* and *Update*, the Kalman filter yields the best estimate of the new state.

HOW TO SMOOTH THE TRAJECTORY USING THE LINEAR KALMAN FILTER

There are two kinds of noise in the Kalman filter according to the basics introduced in previous subsection 2.2.2. From Equations (2.3) to (2.7), we can find the key to achieve smoothing is the parameter K_t, the *Kalman gain*, which is mainly determined by the levels of these noises. So the *Kalman gain* determines how much the predicted value should change in order to become an updated value. To be more precise, it indicates the output value updates based more on the measurements or more on the mathematical model. It means the

larger process uncertainty we set, the less it updates based on the measurement values, the more it learns from the mathematical model, and vice versa. From this point, we can filter out the "noise" by turning the level of process noise and measurement noise. Figure 2.8 gives an example of the smoothing effect of the Kalman filter by setting different noise levels.

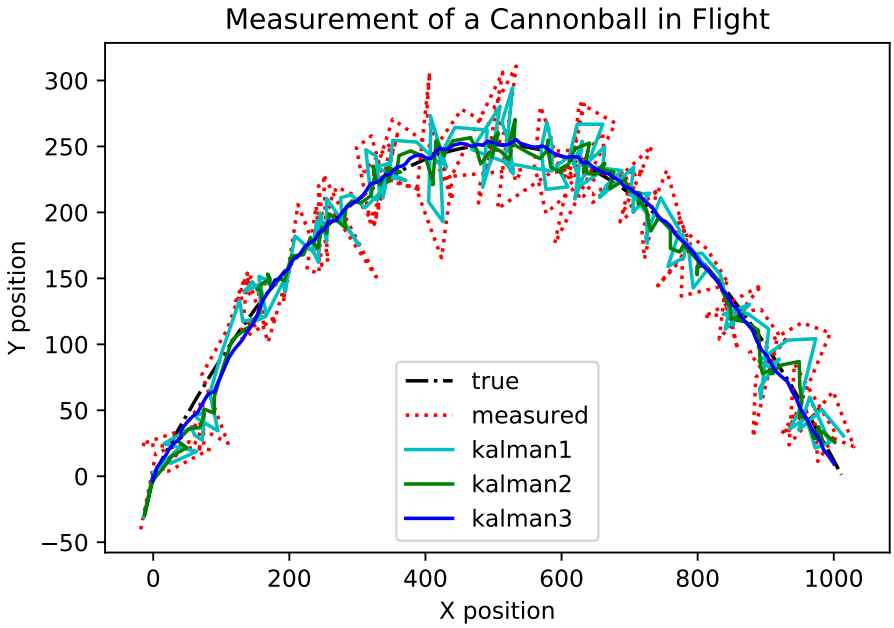

Figure 2.8: **Trajectory Smoothing of a cannonball in flight[16]:** This example is about firing a ball from a cannon at 60-degree angle at a muzzle velocity of 100 units/sec. The physical flying model is easy to describe and the black dash-dot line is the real flight path. A camera also records the ball's positions in a fixed frame rate but with significant measurement error, depicted by the red dotted line. The three lines, "Kalman1" to "Kalman3", show the smoothing effect in three noise level ratios, the measurement noise and process noise ratios are 1,10 and 1000 respectively. It can be noticed that the "kalman3", depicted by the blue line, is smoothed best and is the closest to the real flying trajectory.

But how to smooth the trajectory of a moving hand in our case?

A fundamental assumption for smoothing is that the movement trajectory of a normal hand is smooth instead of trembling. In this case, for a moving hand with tremor, both the tremor signal and the error of estimated hand positions from CPMs are considered as measurement noise. The linear Kalman filter is an optimal estimator in the case that all noise in the random process is Gaussian. Although it is hard to determine the exact probability distribution type of the combined "noise", it is generally assumed that the noise generated by the system or the noise signal received is Gaussian noise under specific frequency bands or constraints.

For the Kalman filter, the more we know the physical model of our situation, the more accurate the estimate of the Kalman filter will be. The physical model is to describe the process mathematically, it is determined by the parameters A_t, B_t and H_t in Equations (2.3) to (2.7). But in our case, it is impossible to find out a universal mathematical model to describe all hand movements of non-identical patients in different tasks. As the tasks with a large motion account for a minority in the *TIM-Tremor* dataset, we produce a stationary physical model by setting the parameters A_t and H_t to identity matrices, B_t to zero matrix. So for one mathematical model, there is a trade-off to set the level of the process noise for both stable tasks and the tasks with large motions.

The levels of two kinds of noise are manually set and tuned for smoothing purpose. We will give the parameter settings of both in section 3.2.

2.3. PHASE-BASED METHOD

An image can be transformed from time domain into frequency domain through two dimensional Fourier transform. The image in the frequency domain contains the magnitude and phase information which have significant analytical value in many image processing applications. Figure 2.9 displays a decomposition ex-

ample of an image. The idea of using phase information frequently appear in many research of computer vision due to its robustness against to noise and lighting changes.

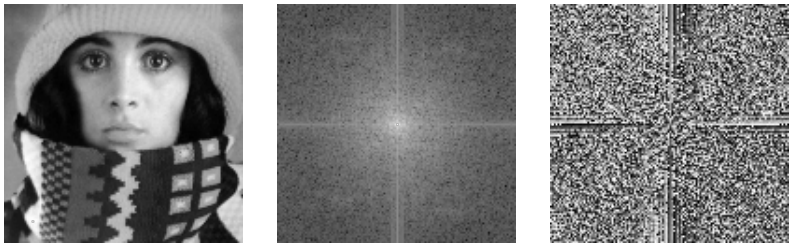

(a) Original image (b) Magnitude spectrum (c) Phase spectrum

Figure 2.9: **The magnitude and phase information of an image[17].**

2.3.1. IMPORTANCE OF PHASE

Figure 2.10 demonstrates the importance of phase information for an image. The phase-only reconstruction preserves features because of the principle of *phase congruency* [18]. It indicates that the image has same phase value at the line and edge positions. Conversely, it is possible to detect lines and edges in an image using the phase information.

Furthermore, according to Fourier phase shift theory, a movement in time domain corresponds to a correlated linear phase shift in the frequency domain. The work in [19] also proves that the phase variations over time are reliable indicators of object movements in consecutive frames. This correspondence can be exploited to represent the movement characteristics of the hand, then to estimate the tremor frequency.

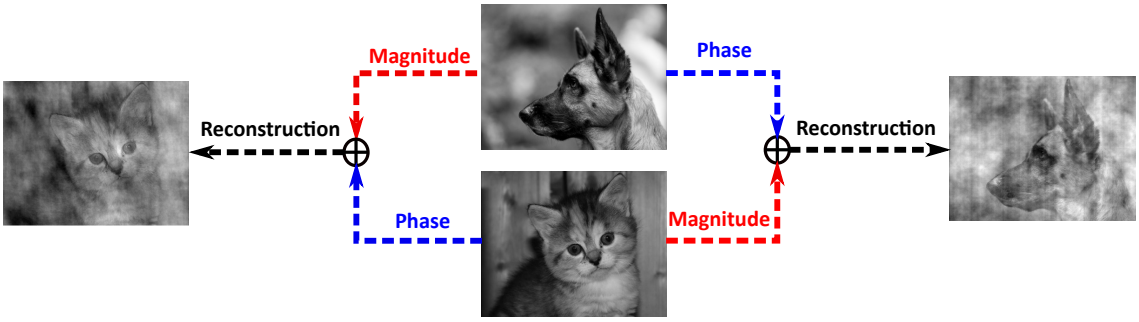

Figure 2.10: **The importance of phase:** Two original images in the middle, a dog and a cat, are decomposed into both magnitude and phase. After swapping their phases, the reconstruction images are shown on the left and right sides. The result demonstrates the importance of phase information for an image.

2.3.2. COMPLEX STEERABLE PYRAMID

The steerable pyramid is a flexible architecture for accurate linear decomposition of an image into the scale and orientation subbands[20]. The image details from decomposition are essential in many image-processing and computer vision applications. The steerable pyramid can calculate kth-order derivatives of the values in an image from multiple directions and scales. It is *steerable* because the constant K can be any positive integer which determines the number of orientation channels. The word *pyramid* refers to the shape of responses on different scales which looks like a pyramid. The structure of steerable pyramid is described in (a) of Figure 2.11. The subsampling procedure for lower-pass sub-band helps us to focus more on the image integrity instead of local image feature in small scale, and the different orientation subbands form a rotation-invariant subspace, leading a tight frame for the whole transform.

In our case, we extract the phase information over multiple orientations and scales by employing the *complex steerable pyramid*, which not only leverages the steerability of the steerable pyramid but also provides phase filters. We call it *complex* because the response of the phase filter in each subband is complex for calculating phase information. Figure 2.11 (b) shows the output phase images of a complex steerable pyramid. Since the hand tremors in videos generally vary in amplitudes and directions, the filters in the complex

steerable pyramid are extremely beneficial to keep the prime tremor characteristic and filter out redundant information and noise.

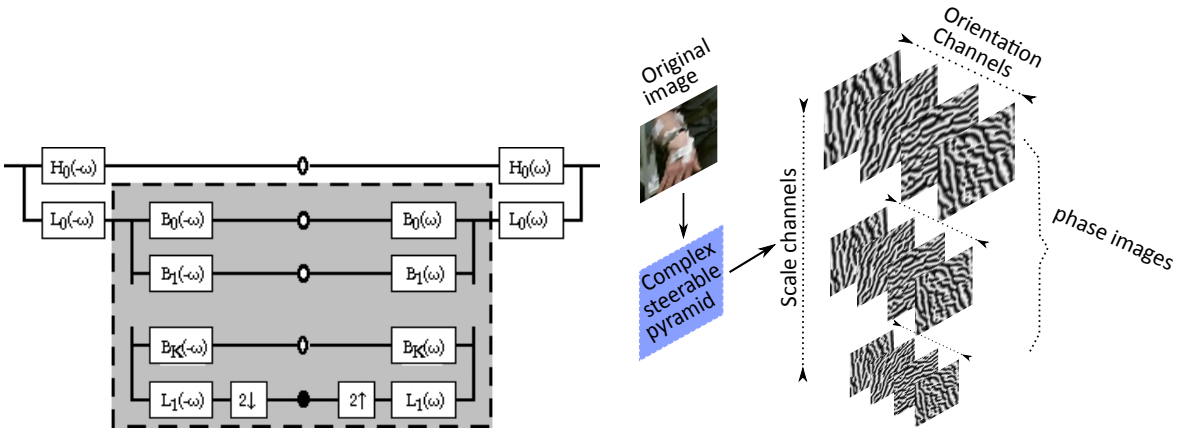

(a) The work structure of steerable pyramid [20] (b) Phase image pyramid

Figure 2.11: **Complex steerable pyramid:** (a) For decomposition, an original image is divided into both low and high pass sub-bands with the filters L_0 and H_0. The low pass sub-band is further decomposed into a set of oriented sub-bands and a lower-pass sub-band L_1. This lower-pass sub-band is sub-sampled by a factor of 2 then turns to a new scale channel. This step is recursive (to become a pyramid) by inserting a copy of the shaded portion of the diagram at the location of the black solid point. The reconstruction part on the right side of the circles can be ignored in our case. (b) We get phase information by employing complex steerable filters on the input image. As the output is complex, we get the phase image pyramid by discarding the amplitude information and only keeping the phase values. A typical pyramid shape is 3 scales and 4 orientations.

3

EXPERIMENT SUPPLEMENTS

In this chapter, we provide more supplements for the experiment part in the scientific paper. First, we present the benchmark for comparison, including an introduction of raw data and how to perform frequency analysis on that. Then we talk about the the parameter selection in the experiment. At the end, more results for multiple tasks are presented, followed by an comparison of four methods in two coordinate systems.

3.1. THE BENCHMARK

As introduced in the scientific paper, we propose four methods with two sets of experiments to perform frequency estimation in videos. We still need a benchmark which contains the "true" tremor frequency to compare the performance of each method. Although the traditional tremor clinical evaluation method is inconvenient, it can accurately record the hand positions over time when with correct operation. We can get the real tremor characteristics of the affected hand with further frequency analysis.

3.1.1. ACCELEROMETER DATA

While recording the videos using the Kinect^{TM} v2 camera, two accelerometers are also attached on a patient's skin for position collection. The first sensor is placed on the back of the hand as depicted in Figure 3.1(a) and sensor 2 is placed on the lower arm (about 5 cm proximal to the wrist joint) in the same direction as sensor 1, but the data from sensor 2 is not used in our case. The location data, as shown in table (b) of 3.1, is then written into a text file through a specific device in preparation for frequency analysis.

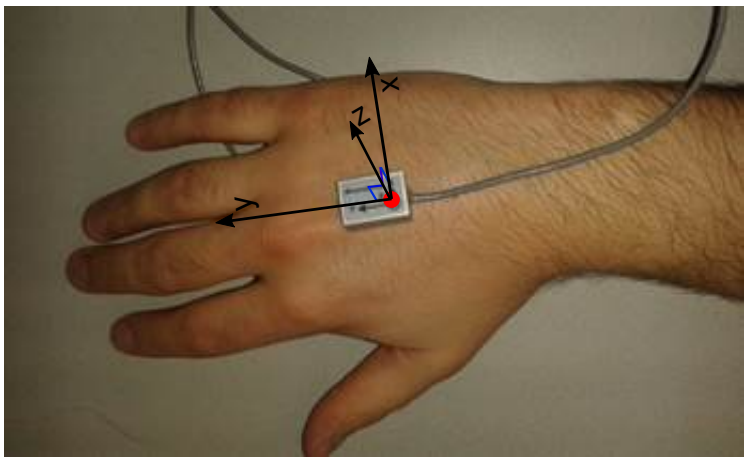

(a) Sensor placed on the hand

S1, X	S1, Y	S1, Z	N/A
-132	427	13	-1
-133	429	11	0
-134	430	11	0
-133	432	10	0
-133	432	9	0
-131	432	9	0
-131	432	7	0
⋮	⋮	⋮	⋮
-129	432	6	0
-128	433	6	0
-128	434	6	0
-127	435	7	0
-126	435	6	1
-126	435	6	1

(b) Recorded data

Figure 3.1: **Benchmark:** Left: The sensor collects the hand position in three axes, i.e., X, Y and Z. In this placement case, the X-axis points to the right side of the arm; the Y-axis points towards the fingers and the Z-axis points away from the skin surface. Right: A slice of recorded data. *S1* refers to the sensor 1. X, Y and Z, each column contains the location change relative to the start point. The fourth column *N/A* is empty. The sensor returns the result every one-thousandth of a second, so the sampling rate is 1000.

3.1.2. FREQUENCY ANALYSIS ON ACCELEROMETER DATA

The recorded locations are samples of the tremor signal in a fixed sampling rate. As a typical frequency range of a hand tremor is between 2Hz and 12Hz which is less than the sampling rate, according to the Nyquist theorem, it is feasible to get the tremor frequency from the position data.

Figure 3.2 illustrates the idea for calculating the tremor frequency from recorded joint locations. A summary of the process is given as follows:

- For signals in each direction, use a 4th-order Butterworth band-pass filter to filter out the frequency components which are lower than 2Hz and higher than 14Hz.
- Remove the direct-current component of the signal by subtracting the average of the signal.
- Perform Short Time Fourier Transform(STFT) with a Tukey window on the signal at each direction. The temporal window size should be the same as the one used by our proposed methods in the scientific paper. The function of STFT and the Tukey window are presented in Equation 3.1 and 3.2:

$$X(m,f) = \sum_{n=-\infty}^{\infty} x(n)\,w(n-m)\,e^{-j2\pi f n} \tag{3.1}$$

$$w(n) = \begin{cases} \frac{1}{2}[1+cos(\pi(\frac{2n}{\alpha(N-1)}-1))] & 0 \le n < \frac{\alpha(N-1)}{2} \\ 1 & \frac{\alpha(N-1)}{2} \le n \le (N-1)(1-\frac{\alpha}{2}) \\ \frac{1}{2}[1+cos(\pi(\frac{2n}{\alpha(N-1)}-\frac{2}{\alpha}+1))] & (N-1)(1-\frac{\alpha}{2}) < n \le (N-1) \end{cases} \tag{3.2}$$

  where $x(n)$ is the signal to be transformed with the discrete time n, $w(n)$ is the Tukey window. f is the frequency axis whose length is related to the width of $w(n)$. m is the window shift, and j is the imaginary unit. In equation 3.2, N is a constant of window size, α is a shape parameter determining the proportion of the window inside the tapered cosine region[21].
- For each direction, compute the power spectrum density(PSD) in each temporal window and add it to the overall PSD in one direction if the PSD follows a "3-σ principle", which is that the maximum of PSD is larger than the mean value plus 3 times of the standard deviation.
- For all directions, take the frequency with the dominant power in PSD as the estimated frequency if it satisfies the "3-σ principle". If not, let the estimated frequency equal to 0, which means no periodicity found in this direction.
- Compute the overall estimated frequency f_O according to Equation 3.3 in [22],

$$f_O = \sqrt{\frac{f_x^2 + f_y^2 + f_z^2}{n}} \tag{3.3}$$

  where f_x, f_y, and f_z are estimated frequencies in three directions respectively, n is the number of frequencies not equal to 0.

3.2. PARAMETER SELECTION

In this section, we give the detail about parameter selection for experiments. Table 3.1 lists some important parameter used in our methods.

Table 3.1: Important parameters for experiments

Property	Value	Property	Value
Window size	61 frames	Overlap	30 frames
Resized frame	654 × 368 px	Box Size	56 px
Filter	3Hz-14Hz	Tukey α	0.25
Kalman Q-level	0.003	Kalman R-level	3
Orientations in pyramid	4	Scales in pyramid	3

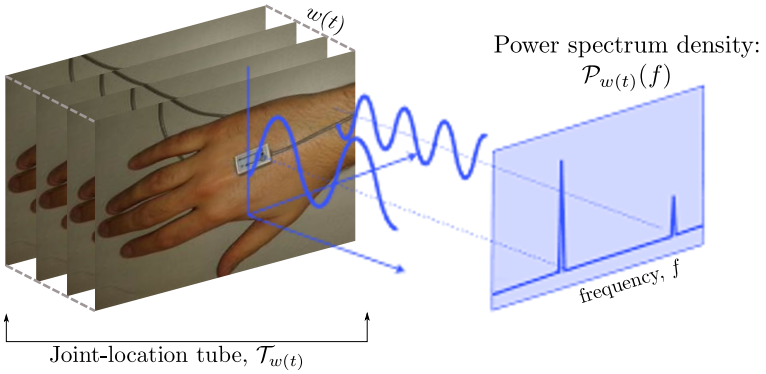

Figure 3.2: **Joint locations to tremor frequency:** In a fixed size temporal window $\varsigma_{w(t)}$, the joint location signal is transformed from time domain to frequency domain by Short Time Fourier Transform(STFT). Based on the power spectrum density $\bar{\omega}_{w(t)}(f)$, the dominant frequency component is picked as estimated tremor frequency.

We select proper parameters empirically or based on control variable experiments. The purpose of parameter selection is to reach trade-offs between two desirable but incompatible features. For example, the window size has a high impact on the estimation accuracy especially for large movement tasks. For an oversized window, big change of the hand shape and frame background makes it difficult for the "tremor detector" to distinguish whether a tremor exists or just full of noise. While a small window size also results in a small resolution of the spectrum which also limits the accuracy. We made an additional test on window size on a large movement task *Top_nose_right* and calculated the mean square error between estimated frequency and benchmark. The MSE curve is shown in Figure 3.3. We also rescale the frame size to speed up the pose estimation module, which inevitably leads to losing a small part of the image details.

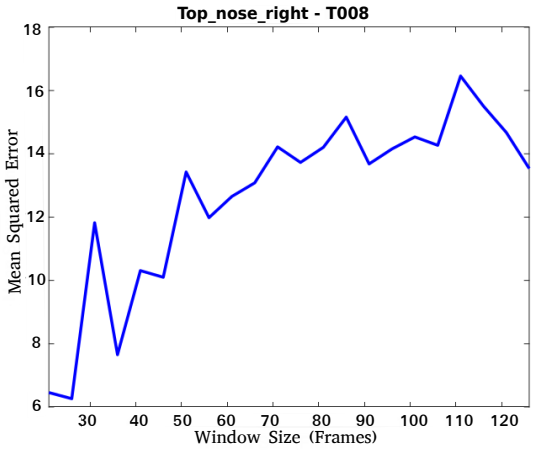

Figure 3.3: **MSE vs Window Size[12]:** The mean square error curve indicates an overall up trend with the window size.

3.3. MORE RESULTS

In the scientific paper, we only present two representative experiment results due to limited space, more figures of experiment results on different tasks are presented in (a) to (d) in Figure 3.4.

We totally propose four methods in two coordinate systems in the scientific paper, the mean absolute error of four experiment variants for all tasks in the *TIM-Tremor* dataset is shown in Figure 3.5. From the results, we can see the Eulerian approaches are more accurate than the Lagrangian methods in most of the tasks. The *Euler_phase* approach achieves small absolute error in some tasks, such as task *counting* in (a) of Figure 3.4 and task *Top-top* in (b) of Figure 3.4, where the hand is overall stable except with a tremor. The Lagrangian methods perform better than the Eulerian in some tasks with big motion, such like *Top-top* in (d) of Figure 3.4, this is because the change of hand shape and background does not influence the Lagrangian methods while the Eulerian approaches assume the hand shape does not change over time. The use of phase information also improves the estimation performance in the Eulerian approaches thanks to the benefits

from the *complex steerable pyramid*. The frequency estimation results of all tasks are listed in tables A.1 to A.21 of appendix A.

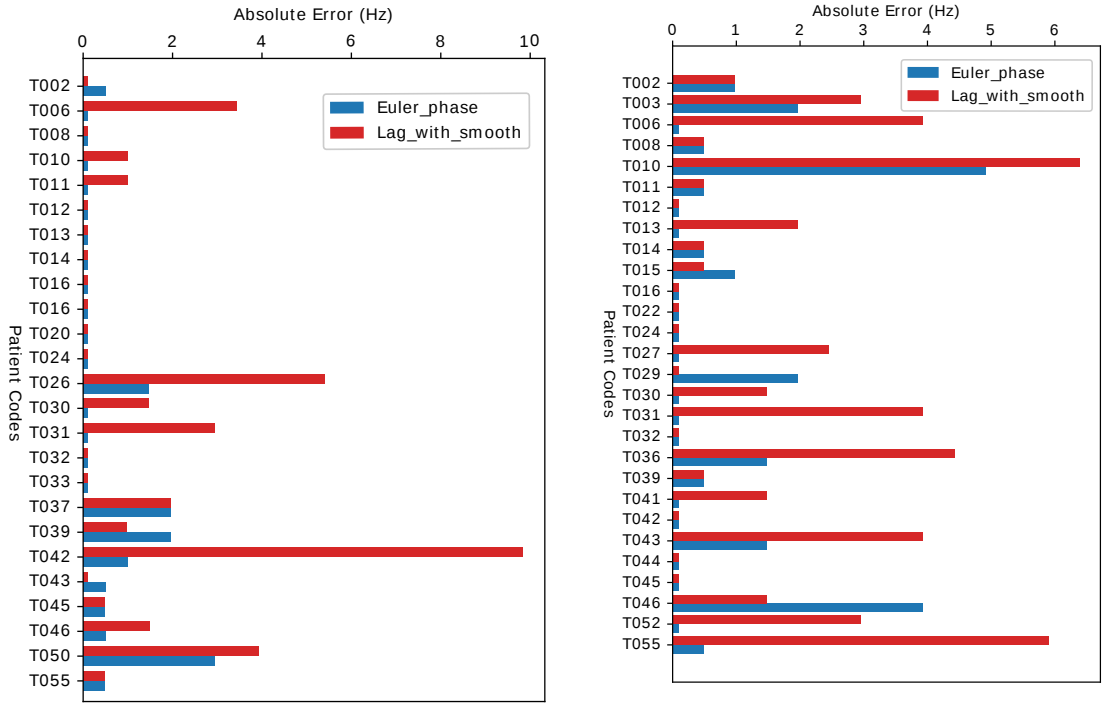

(a) *Counting* (b) *Top-top*

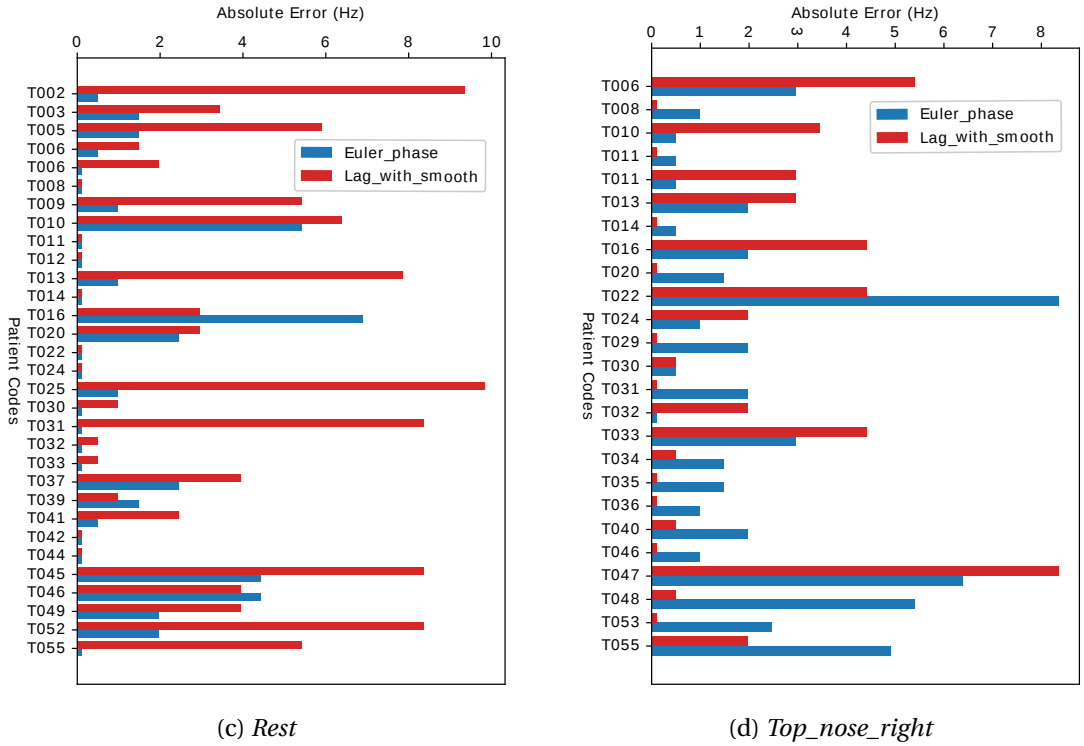

(c) *Rest* (d) *Top_nose_right*

Figure 3.4: **More results on different tasks:** Here we present four more results of the Eulerian method and the Lagrangian method (lower is better). In (a) (b) and (c), the Eulerian method performs better; but in (d), the big motion causes a performance degradation for the Eulerian method.

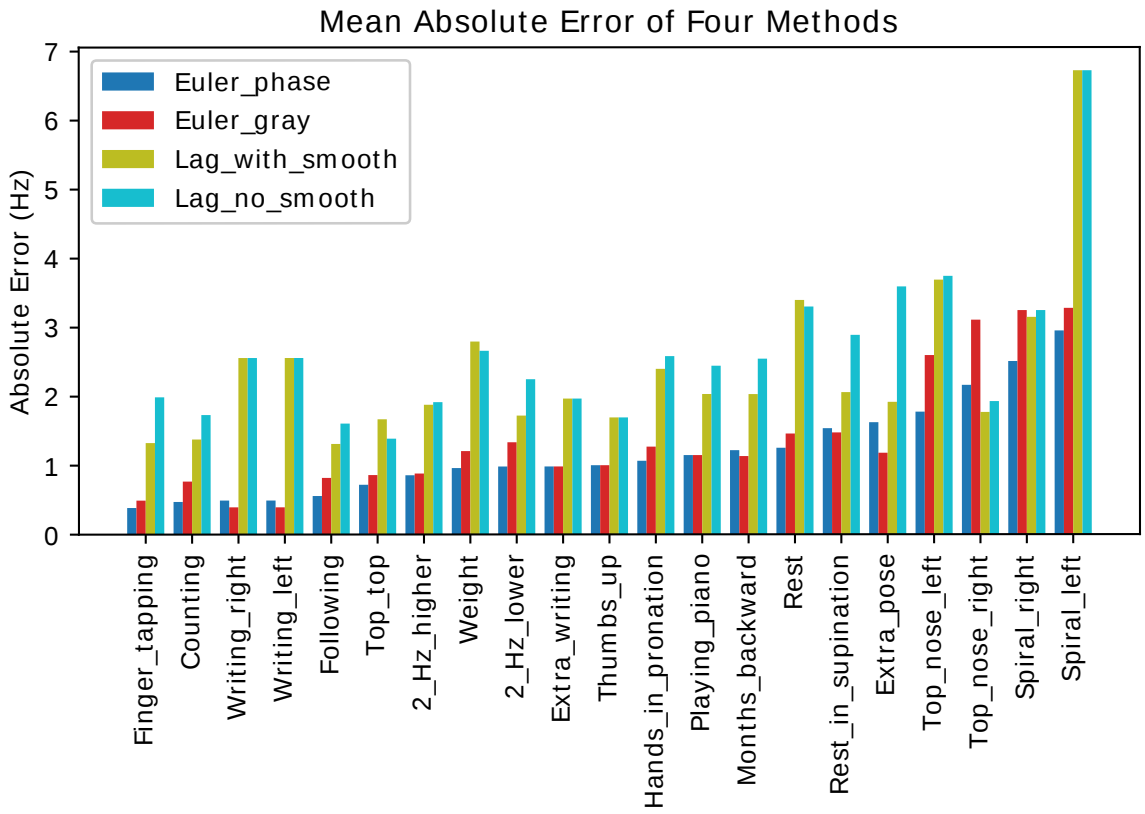

Figure 3.5: **Mean absolute error of four methods:** We report mean absolute error on all recorded tasks (lower is better). Here we take average only on the videos where periodicity is detected in the benchmark. On average the Eulerian based methods get smaller error than the Lagrangian methods, and the phase information and trajectory smoothing also help to achieve better performance in totality.

BIBLIOGRAPHY

[1] A. Cappello, A. Leardini, M. G. Benedetti, R. Liguori, and A. Bertani, *Application of stereophotogrammetry to total body three-dimensional analysis of human tremor,* IEEE Transactions on Rehabilitation Engineering **5**, 388 (1997).

[2] C. W. Hess and S. L. Pullman, *Tremor: clinical phenomenology and assessment techniques,* Tremor and other hyperkinetic movements **2** (2012).

[3] A. Beuter, L. Glass, M. C. Mackey, and M. S. Titcombe, *Nonlinear dynamics in physiology and medicine* (2003).

[4] J. Spehr, *On hierarchical models for visual recognition and learning of objects, scenes, and activities.*, Ph.D. thesis, Springer (2013).

[5] M. Andriluka, L. Pishchulin, P. Gehler, and B. Schiele, *2d human pose estimation: New benchmark and state of the art analysis,* in *Proceedings of the IEEE Conference on computer Vision and Pattern Recognition* (2014) pp. 3686–3693.

[6] J. Carreira, P. Agrawal, K. Fragkiadaki, and J. Malik, *Human pose estimation with iterative error feedback,* in *Proceedings of the IEEE conference on computer vision and pattern recognition* (2016) pp. 4733–4742.

[7] A. Bulat and G. Tzimiropoulos, *Human pose estimation via convolutional part heatmap regression,* in *European Conference on Computer Vision* (Springer, 2016) pp. 717–732.

[8] S.-E. Wei, V. Ramakrishna, T. Kanade, and Y. Sheikh, *Convolutional pose machines,* in *Proceedings of the IEEE Conference on Computer Vision and Pattern Recognition* (2016) pp. 4724–4732.

[9] J. Kooij and J. van Gemert, *Depth-aware motion magnification,* in *European Conference on Computer Vision* (Springer, 2016) pp. 467–482.

[10] N. Wadhwa, M. Rubinstein, F. Durand, and W. T. Freeman, *Phase-based video motion processing,* SIGGRAPH **32**, 80 (2013).

[11] V. Ramakrishna, D. Munoz, M. Hebert, A. J. Bagnell, and Y. Sheikh, *Pose machines: Articulated pose estimation via inference machines,* in *ECCV* (2014).

[12] X. Li, *Pathological tremor detection from video,* (2017).

[13] S. Johnson and M. Everingham, *Learning effective human pose estimation from inaccurate annotation,* in *Computer vision and pattern recognition (CVPR), 2011 IEEE conference on* (IEEE, 2011) pp. 1465–1472.

[14] R. Faragher *et al., Understanding the basis of the kalman filter via a simple and intuitive derivation,* IEEE Signal processing magazine **29**, 128 (2012).

[15] Wikipedia contributors, *Kalman filter — Wikipedia, the free encyclopedia,* (2018), [Online; accessed 6-August-2018].

[16] G. Czerniak, *Greg czerniak's website on the linear Kalman filters,* (2018), [Online; accessed: 2018-08-15].

[17] I.T. Young, J.J. Gerbrands, L.J. van Vliet, *Image processing fundamentals,* (2018), [Online; accessed 12-August-2018].

[18] M. C. Morrone and D. Burr, *Feature detection in human vision: A phase-dependent energy model,* Proc. R. Soc. Lond. B **235**, 221 (1988).

[19] D. J. Fleet and A. D. Jepson, *Computation of component image velocity from local phase information,* International journal of computer vision **5**, 77 (1990).

[20] E. P. Simoncelli and W. T. Freeman, *The steerable pyramid: A flexible architecture for multi-scale derivative computation,* in *Image Processing, 1995. Proceedings., International Conference on*, Vol. 3 (IEEE, 1995) pp. 444–447.

[21] F. J. Harris, *On the use of windows for harmonic analysis with the discrete fourier transform,* Proceedings of the IEEE **66**, 51 (1978).

[22] A. Salarian, H. Russmann, C. Wider, P. R. Burkhard, F. J. Vingerhoets, and K. Aminian, *Quantification of tremor and bradykinesia in parkinson's disease using a novel ambulatory monitoring system,* IEEE Transactions on Biomedical Engineering **54**, 313 (2007).

A

APPENDIX

A.1. FREQUENCY EVALUATION RESULTS

Table A.1 to Table A.20 list all frequency estimation results of all tasks for different patients. In each table, the first column records the code of patient, and the second column lists ground truth frequencies analyzed from the accelerometer data. The third column to the sixth column records the estimated frequencies from videos of four methods respectively. For all the tables, we also include the patient videos in which no periodicity is detected in the benchmark.

Table A.1: Frequency estimation results for all patients in the task *Extra_pose*.

Patient	Benchmark(Hz)	Euler_phase(Hz)	Euler_gray(Hz)	Lag_with_smooth(Hz)	Lag_no_smooth(Hz)
T010	8.362027	5.409836	5.409836	3.442623	3.442623
T055	8.362027	8.360656	8.360656	7.377049	1.967213
T054	3.443187	3.442623	3.442623	2.950820	1.967213
T018	2.951303	3.442623	0.000000	1.967213	1.967213
T018	5.902607	3.934426	3.442623	2.950820	2.950820
T022	4.426955	7.868852	4.918033	7.868852	7.868852
T047	2.459420	3.934426	3.934426	1.967213	1.967213
T045	5.410723	5.901639	5.901639	5.409836	5.409836
T039	4.426955	5.901639	5.901639	1.967213	1.967213
T047	2.459420	4.426230	4.918033	2.459016	2.459016
T050	6.394491	3.934426	4.426230	3.934426	0.000000
T003	5.410723	3.934426	3.934426	4.426230	4.426230
T048	6.394491	3.934426	3.934426	2.459016	2.459016
T039	5.902607	3.934426	5.901639	1.967213	1.967213
T047	9.345794	3.442623	0.000000	1.967213	1.967213
T021	5.902607	4.426230	4.426230	2.459016	2.459016
T029	2.459420	3.934426	3.934426	1.967213	1.967213
T031	5.902607	3.934426	5.901639	6.885246	1.967213
T045	4.918839	5.409836	5.409836	5.409836	5.409836
T045	5.902607	5.409836	5.901639	2.459016	2.459016
T052	6.886375	3.442623	0.000000	4.426230	0.000000
T034_2	4.918839	10.819672	10.819672	10.819672	10.819672

Table A.2: Frequency estimation results for all patients in the task *2_hz_higher*.

Patient	Benchmark(Hz)	Euler_phase(Hz)	Euler_gray(Hz)	Lag_with_smooth(Hz)	Lag_no_smooth(Hz)
T001	2.951303	2.950820	4.426230	2.950820	2.950820
T002	3.443187	3.934426	3.934426	2.950820	2.459016
T003	3.935071	4.918033	4.426230	3.442623	1.967213
T005	4.426955	3.934426	9.344262	6.393443	6.393443
T006	5.410723	4.918033	5.409836	2.950820	5.409836
T007	4.918839	3.934426	3.934426	1.967213	1.967213
T009	3.443187	3.442623	3.442623	3.442623	3.442623
T010	4.426955	4.426230	4.426230	3.442623	3.442623
T011	9.345794	4.918033	4.918033	4.918033	4.918033
T012	4.918839	4.918033	4.918033	5.409836	5.409836
T013	4.918839	4.918033	4.918033	4.918033	2.950820
T014	5.410723	5.901639	5.901639	5.901639	5.901639
T015	6.886375	6.885246	6.393443	3.934426	3.934426
T016	5.902607	5.901639	5.901639	8.360656	8.360656
T017	4.918839	4.918033	5.409836	2.459016	2.459016
T018	4.918839	4.918033	4.918033	2.950820	2.950820
T019	5.902607	5.901639	5.901639	3.442623	5.901639
T020	6.886375	7.377049	7.377049	7.377049	7.377049
T021	5.410723	4.426230	6.393443	1.967213	1.967213
T022	4.426955	4.426230	4.426230	3.934426	14.262295
T023	5.902607	5.901639	5.901639	5.901639	5.901639
T026	5.410723	5.409836	4.918033	2.459016	2.459016
T027	5.902607	5.409836	7.377049	6.393443	6.393443
T028	5.410723	5.409836	5.409836	14.754098	14.262295
T029	3.443187	3.442623	3.442623	3.442623	3.442623
T030	4.426955	4.918033	4.918033	4.918033	4.918033
T031	5.902607	3.934426	3.934426	2.950820	2.950820
T032	4.426955	4.918033	4.918033	3.442623	3.442623
T033	5.902607	3.934426	3.934426	1.967213	1.967213
T034	4.918839	10.327869	10.327869	2.459016	2.459016
T035	2.951303	2.950820	2.950820	2.950820	2.950820
T036	7.378259	4.426230	4.426230	2.950820	2.950820
T037	6.886375	3.934426	3.934426	3.442623	3.442623
T038	4.918839	5.409836	5.409836	4.918033	5.409836
T039	6.394491	3.442623	3.442623	3.442623	3.442623
T040	5.410723	5.409836	5.409836	2.459016	5.409836
T041	5.902607	6.393443	6.393443	10.819672	6.393443
T042	5.410723	3.442623	7.377049	4.918033	4.918033
T043	4.918839	6.393443	6.393443	3.442623	3.442623
T044	4.918839	4.918033	4.918033	4.918033	4.918033
T045	4.918839	4.918033	4.918033	4.918033	4.918033
T046	6.394491	6.393443	6.393443	5.901639	5.901639
T047	2.951303	11.311475	4.918033	2.950820	2.950820
T050	6.394491	4.426230	4.426230	4.426230	4.426230
T051	2.459420	9.344262	9.344262	2.950820	2.950820
T052	5.410723	5.409836	5.409836	5.409836	5.409836
T053	4.426955	4.426230	4.918033	12.295082	12.295082
T055	8.362027	10.327869	10.327869	10.327869	10.327869

Table A.3: Frequency estimation results for all patients in the task *2_hz_lower*.

Patient	Benchmark(Hz)	Euler_phase(Hz)	Euler_gray(Hz)	Lag_with_smooth(Hz)	Lag_no_smooth(Hz)
T001	1.967536	4.426230	4.426230	2.459016	2.459016
T002	5.410723	3.934426	4.426230	2.459016	2.459016
T003	4.426955	7.377049	4.426230	2.950820	8.360656
T005	3.443187	5.409836	5.409836	1.967213	1.967213
T006	5.410723	2.459016	3.442623	2.459016	2.459016
T007	4.426955	4.918033	4.918033	2.950820	2.459016
T008	5.410723	5.409836	5.409836	5.409836	5.409836
T009	6.886375	3.442623	3.442623	2.950820	2.950820
T010	3.443187	3.442623	3.442623	2.950820	2.950820
T011	5.410723	3.934426	5.409836	2.459016	2.459016
T012	4.918839	4.918033	4.918033	4.918033	4.918033
T013	4.426955	4.426230	4.426230	4.426230	2.950820
T014	5.902607	5.901639	5.901639	6.885246	4.918033
T015	6.394491	5.901639	5.901639	3.442623	3.442623
T016	5.410723	5.409836	5.901639	2.950820	2.950820
T017	2.951303	3.442623	4.918033	4.918033	4.918033
T018	4.918839	4.918033	4.918033	4.426230	4.918033
T019	12.788982	4.426230	4.426230	4.426230	4.426230
T020	3.935071	3.934426	3.934426	3.934426	3.934426
T021	2.951303	3.934426	3.934426	2.950820	2.950820
T022	4.426955	4.426230	4.426230	4.426230	4.426230
T023	8.362027	2.950820	3.442623	2.950820	2.950820
T024	5.410723	5.409836	5.409836	5.409836	5.409836
T026	3.935071	4.426230	3.934426	14.262295	14.262295
T027	1.967536	4.426230	4.426230	2.459016	2.459016
T028	2.951303	3.442623	5.409836	2.950820	2.950820
T029	4.426955	4.426230	4.426230	4.426230	4.426230
T030	4.426955	4.426230	4.426230	1.967213	1.967213
T031	5.902607	2.950820	4.426230	2.950820	1.967213
T032	4.426955	4.918033	4.918033	2.459016	2.459016
T033	5.902607	4.426230	5.901639	2.459016	2.459016
T034	3.443187	5.901639	12.295082	2.459016	2.459016
T035	2.459420	2.950820	2.950820	2.950820	2.950820
T036	3.443187	3.934426	12.295082	2.459016	2.459016
T037	2.951303	3.934426	3.934426	2.950820	2.950820
T038	3.443187	4.426230	7.868852	3.934426	14.262295
T039	6.394491	3.442623	3.442623	3.442623	3.442623
T040	3.935071	3.934426	3.934426	3.934426	1.967213
T041	5.902607	5.901639	5.901639	5.901639	4.426230
T042	5.410723	3.442623	3.934426	3.442623	3.442623
T043	2.951303	7.868852	7.868852	8.852459	8.852459
T044	4.918839	4.918033	4.918033	2.459016	2.459016
T045	4.918839	4.918033	4.918033	4.918033	5.409836
T046	6.394491	6.393443	6.885246	6.393443	6.393443
T047	3.443187	3.442623	3.442623	3.442623	3.442623
T050	1.967536	3.934426	3.442623	1.967213	1.967213
T051	3.443187	4.426230	4.426230	3.934426	3.934426
T052	6.394491	5.901639	5.901639	2.459016	2.459016
T053	3.935071	3.934426	4.426230	3.442623	3.442623
T055	7.870143	4.918033	4.918033	3.934426	3.934426

Table A.4: Frequency estimation results for all patients in the task *Counting*.

Patient	Benchmark(Hz)	Euler_phase(Hz)	Euler_gray(Hz)	Lag_with_smooth(Hz)	Lag_no_smooth(Hz)
T001	2.45942	3.442623	3.934426	2.459016	2.459016
T002	4.426955	3.934426	5.409836	4.42623	4.42623
T003	5.410723	4.918033	9.836066	2.459016	2.459016
T005	3.443187	3.934426	3.934426	2.459016	2.459016
T006	6.394491	6.393443	3.442623	2.95082	2.459016
T007	7.378259	6.885246	4.42623	2.95082	2.95082
T008	5.410723	5.409836	5.409836	5.409836	5.409836
T009	6.886375	5.409836	3.934426	3.442623	3.442623
T010	6.886375	6.885246	4.42623	5.901639	3.934426
T011	4.918839	4.918033	4.918033	3.934426	2.95082
T012	4.918839	4.918033	4.918033	4.918033	4.918033
T013	4.426955	4.42623	3.934426	4.42623	1.967213
T014	5.410723	5.409836	5.409836	5.409836	5.409836
T015	7.870143	3.934426	7.868852	2.459016	2.459016
T016	5.902607	5.901639	5.901639	5.901639	5.901639
T017	6.394491	3.934426	3.934426	2.95082	2.95082
T018	3.443187	4.918033	5.409836	2.95082	2.95082
T019	6.394491	4.918033	3.442623	2.95082	8.360656
T020	6.886375	6.885246	6.885246	6.885246	6.885246
T021	2.45942	3.442623	3.934426	2.459016	2.459016
T022	4.918839	4.42623	4.42623	3.934426	4.42623
T023	3.443187	4.918033	8.852459	2.95082	2.95082
T024	5.410723	5.409836	5.409836	5.409836	5.409836
T026	8.85391	10.327869	3.934426	14.262295	14.262295
T027	2.45942	4.42623	4.918033	2.459016	2.459016
T028	2.951303	4.918033	7.868852	14.262295	14.262295
T029	3.443187	3.442623	3.442623	3.442623	3.442623
T030	4.426955	4.42623	4.42623	2.95082	2.95082
T031	5.410723	5.409836	5.409836	2.459016	2.459016
T032	5.410723	5.409836	5.409836	5.409836	5.409836
T033	5.902607	5.901639	5.901639	5.901639	5.901639
T034	9.345794	3.934426	4.42623	2.459016	2.459016
T035	4.426955	4.918033	5.901639	2.95082	2.95082
T036	7.378259	3.442623	3.934426	2.459016	1.967213
T037	5.410723	3.442623	7.868852	3.442623	3.442623
T038	2.951303	3.934426	13.278689	5.409836	5.409836
T039	5.410723	3.442623	5.409836	6.393443	6.393443
T040	2.951303	3.442623	3.442623	1.967213	1.967213
T041	4.426955	3.934426	4.42623	9.344262	2.95082
T042	4.918839	3.934426	3.934426	14.754098	14.754098
T043	5.410723	4.918033	5.409836	5.409836	5.409836
T044	3.935071	3.934426	3.934426	14.262295	14.262295
T045	4.426955	4.918033	4.918033	4.918033	4.918033
T046	6.394491	5.901639	5.901639	4.918033	1.967213
T047	2.45942	3.442623	3.442623	2.459016	2.459016
T050	6.394491	3.442623	3.934426	2.459016	2.459016
T051	5.902607	3.934426	3.442623	2.459016	2.459016
T052	5.410723	5.409836	5.409836	5.409836	5.901639
T053	2.45942	3.442623	3.442623	2.95082	2.95082
T054	7.870143	3.442623	3.934426	2.459016	3.442623
T055	7.378259	7.868852	7.868852	7.868852	7.868852
T042_2	5.410723	3.442623	4.42623	2.459016	3.442623
T016_2	4.426955	4.42623	4.42623	4.42623	4.42623
T018_2	4.918839	4.42623	4.42623	14.262295	14.262295

Table A.5: Frequency estimation results for all patients in the task *Finger_tapping*.

Patient	Benchmark(Hz)	Euler_phase(Hz)	Euler_gray(Hz)	Lag_with_smooth(Hz)	Lag_no_smooth(Hz)
T001	2.459420	3.442623	3.934426	2.459016	2.459016
T002	4.918839	4.918033	4.918033	5.409836	5.409836
T003	3.443187	3.934426	3.934426	3.934426	3.934426
T005	5.902607	4.426230	5.901639	2.459016	2.459016
T006	5.410723	5.901639	5.409836	2.459016	2.459016
T007	2.459420	3.934426	3.934426	2.950820	2.950820
T008	5.410723	5.409836	5.409836	5.409836	5.409836
T009	5.902607	3.442623	3.442623	3.442623	3.442623
T010	3.935071	3.442623	3.934426	2.459016	2.459016
T011	5.410723	3.442623	3.442623	3.442623	3.442623
T012	4.918839	4.918033	4.918033	4.918033	4.918033
T013	4.426955	4.426230	4.426230	4.426230	4.426230
T014	5.410723	5.901639	5.409836	5.901639	5.901639
T015	7.870143	5.409836	5.409836	3.442623	3.442623
T016	5.902607	5.901639	5.901639	5.901639	2.950820
T017	6.886375	4.426230	4.426230	4.426230	4.426230
T018	3.935071	4.426230	3.934426	2.950820	2.950820
T019	2.951303	2.950820	3.442623	2.950820	3.442623
T020	2.951303	3.442623	3.442623	2.950820	2.950820
T021	6.394491	4.918033	3.934426	2.950820	2.950820
T022	4.426955	4.918033	4.918033	4.918033	4.918033
T023	4.426955	4.426230	4.426230	3.934426	3.442623
T024	5.410723	5.409836	5.409836	5.409836	5.409836
T025	4.426955	4.426230	4.918033	2.950820	2.950820
T026	8.853910	10.327869	3.934426	3.934426	14.262295
T027	5.902607	4.918033	4.918033	2.459016	2.459016
T028	7.378259	5.409836	5.409836	1.967213	1.967213
T029	3.443187	3.442623	3.442623	3.442623	3.442623
T030	4.426955	4.426230	4.426230	4.426230	4.426230
T031	5.902607	3.934426	3.934426	2.459016	2.950820
T032	4.918839	4.918033	4.918033	4.918033	4.918033
T033	5.902607	5.901639	5.901639	5.901639	5.901639
T034	8.853910	3.934426	3.934426	2.459016	2.459016
T035	3.443187	3.442623	3.442623	3.442623	3.442623
T036	7.378259	3.934426	3.934426	1.967213	1.967213
T037	2.951303	3.934426	6.393443	3.442623	14.262295
T038	2.951303	6.885246	7.868852	2.950820	2.950820
T039	4.426955	4.426230	4.918033	2.459016	2.459016
T040	2.459420	3.934426	3.934426	2.950820	2.950820
T041	6.394491	4.426230	7.377049	14.262295	14.262295
T042	2.459420	3.934426	6.393443	2.459016	2.459016
T043	5.902607	5.901639	5.901639	14.262295	14.262295
T044	2.459420	3.442623	3.442623	1.967213	1.967213
T045	4.918839	5.409836	5.409836	5.409836	5.409836
T046	5.902607	5.901639	5.901639	6.393443	3.442623
T047	2.459420	3.442623	3.442623	3.442623	2.950820
T050	6.886375	3.934426	3.934426	2.950820	2.459016
T051	5.902607	3.442623	13.770492	13.278689	13.278689
T052	5.410723	5.409836	5.409836	5.409836	5.409836
T053	2.951303	3.934426	3.934426	2.459016	2.459016
T054	6.394491	3.442623	3.934426	2.459016	2.459016
T055	8.362027	8.360656	7.868852	4.426230	4.426230
T020_2	3.935071	4.426230	4.426230	14.262295	14.262295
T020_3	1.967536	4.426230	4.426230	1.967213	1.967213
T041_2	8.362027	5.409836	4.918033	5.409836	5.409836

Table A.6: Frequency estimation results for all patients in the task *Following*.

Patient	Benchmark(Hz)	Euler_phase(Hz)	Euler_gray(Hz)	Lag_with_smooth(Hz)	Lag_no_smooth(Hz)
T001	2.459420	3.934426	5.409836	2.950820	2.950820
T002	4.918839	4.918033	4.918033	2.950820	2.950820
T003	2.951303	3.442623	7.868852	1.967213	1.967213
T005	2.951303	3.934426	3.442623	2.459016	2.459016
T006	2.459420	3.442623	0.000000	1.967213	1.967213
T007	2.459420	3.934426	3.934426	2.950820	4.426230
T009	6.886375	3.442623	3.442623	2.459016	1.967213
T010	7.378259	3.934426	3.934426	2.459016	1.967213
T011	2.951303	4.426230	0.000000	2.459016	2.459016
T012	4.918839	3.934426	3.934426	2.459016	2.459016
T013	4.426955	4.426230	4.426230	2.950820	2.459016
T014	4.918839	4.918033	4.918033	4.918033	4.918033
T015	2.459420	3.934426	0.000000	1.967213	1.967213
T016	5.902607	5.409836	5.901639	1.967213	1.967213
T017	2.951303	3.934426	4.426230	2.459016	2.950820
T018	2.459420	3.442623	3.442623	1.967213	1.967213
T019	2.459420	3.442623	9.836066	2.459016	1.967213
T020	2.951303	3.442623	3.442623	4.426230	4.426230
T021	2.459420	3.442623	4.918033	2.459016	2.459016
T022	2.459420	3.934426	3.934426	3.442623	3.442623
T023	2.459420	3.442623	3.934426	1.967213	1.967213
T024	4.918839	3.934426	4.918033	4.918033	4.918033
T026	2.459420	10.327869	3.934426	1.967213	1.967213
T027	2.459420	3.442623	3.442623	1.967213	1.967213
T028	2.459420	3.934426	3.934426	2.459016	14.262295
T029	4.426955	3.442623	4.918033	1.967213	1.967213
T030	4.426955	4.426230	4.426230	2.459016	2.950820
T031	2.459420	3.934426	5.901639	2.950820	1.967213
T032	4.426955	3.442623	3.442623	1.967213	1.967213
T034	1.967536	3.442623	3.934426	2.459016	1.967213
T035	2.459420	3.442623	0.000000	2.459016	2.459016
T036	2.951303	3.934426	3.442623	2.459016	2.459016
T037	2.459420	3.442623	3.442623	2.459016	2.459016
T038	2.459420	3.442623	3.934426	2.459016	2.459016
T039	5.410723	3.442623	0.000000	1.967213	1.967213
T040	2.951303	3.442623	3.442623	2.459016	2.459016
T041	3.935071	3.442623	6.885246	1.967213	1.967213
T042	5.410723	3.442623	3.934426	2.459016	2.459016
T043	2.951303	3.442623	3.934426	14.262295	14.262295
T044	2.459420	3.442623	0.000000	1.967213	1.967213
T045	5.410723	5.409836	5.409836	5.409836	5.409836
T046	5.410723	5.409836	5.409836	1.967213	1.967213
T047	2.951303	3.442623	3.442623	2.950820	2.950820
T050	2.459420	3.442623	3.934426	2.950820	1.967213
T051	2.459420	3.442623	3.442623	1.967213	1.967213
T052	5.410723	5.409836	0.000000	5.409836	1.967213
T053	2.459420	3.442623	3.442623	2.459016	2.459016
T054	6.886375	3.442623	3.934426	1.967213	1.967213
T055	7.870143	7.868852	7.868852	1.967213	1.967213

Table A.7: Frequency estimation results for all patients in the task *Hands_in_pronation*.

Patient	Benchmark(Hz)	Euler_phase(Hz)	Euler_gray(Hz)	Lag_with_smooth(Hz)	Lag_no_smooth(Hz)
T001	6.394491	4.426230	6.393443	2.950820	2.950820
T002	4.918839	4.918033	4.918033	4.426230	4.918033
T003	6.394491	3.934426	11.803279	3.934426	3.442623
T004	4.918839	3.934426	7.868852	4.426230	2.950820
T005	6.394491	10.819672	12.786885	10.819672	10.819672
T006	6.394491	5.901639	4.426230	7.868852	7.868852
T007	2.459420	4.918033	5.901639	3.442623	2.459016
T008	5.410723	5.409836	5.409836	5.409836	5.409836
T009	7.378259	8.360656	8.360656	1.967213	2.459016
T010	8.362027	3.934426	3.934426	1.967213	1.967213
T011	4.918839	5.409836	5.409836	5.409836	5.409836
T012	6.394491	3.934426	3.934426	5.409836	5.409836
T013	4.918839	4.918033	4.918033	4.918033	4.918033
T014	5.410723	5.901639	5.901639	5.901639	5.901639
T015	7.870143	5.409836	4.426230	2.950820	2.950820
T016	5.902607	5.901639	5.901639	2.950820	2.950820
T017	7.378259	3.442623	3.442623	1.967213	1.967213
T018	7.378259	3.442623	3.442623	3.442623	3.442623
T019	8.853910	3.442623	4.426230	3.442623	3.442623
T020	2.459420	11.803279	11.803279	14.262295	2.459016
T021	6.394491	5.901639	6.885246	2.459016	2.459016
T022	8.853910	3.934426	3.934426	14.754098	14.754098
T023	8.853910	4.426230	4.918033	14.262295	2.459016
T024	5.410723	5.409836	6.393443	3.442623	3.442623
T025	4.426955	3.934426	3.934426	8.852459	8.852459
T026	9.345794	10.327869	4.918033	1.967213	1.967213
T027	5.410723	4.918033	4.918033	4.426230	2.950820
T028	7.378259	4.918033	5.409836	2.459016	2.459016
T029	4.918839	4.918033	4.918033	4.426230	4.426230
T030	4.426955	4.426230	4.426230	2.950820	2.950820
T031	5.902607	5.901639	5.901639	3.442623	3.442623
T032	5.410723	5.901639	5.409836	4.918033	4.918033
T033	5.902607	5.901639	5.901639	1.967213	1.967213
T034	10.329562	3.934426	3.934426	2.459016	2.459016
T035	5.902607	3.442623	5.409836	3.442623	2.459016
T036	2.459420	2.950820	5.901639	2.950820	2.950820
T037	5.902607	3.934426	0.000000	2.950820	2.950820
T038	7.870143	5.409836	6.393443	5.409836	6.393443
T039	5.902607	4.918033	4.918033	2.950820	2.950820
T040	2.951303	3.934426	3.934426	2.459016	2.459016
T041	7.870143	3.934426	7.868852	6.393443	1.967213
T042	5.410723	5.409836	5.409836	6.393443	6.393443
T043	5.902607	4.426230	4.426230	2.950820	2.950820
T044	5.902607	4.426230	4.918033	2.459016	2.459016
T045	4.918839	4.918033	4.918033	4.918033	4.918033
T046	6.394491	10.327869	10.327869	2.459016	2.459016
T047	2.459420	3.934426	3.934426	1.967213	1.967213
T048	2.459420	10.327869	4.918033	8.852459	8.852459
T049	6.394491	3.442623	3.442623	2.950820	2.950820
T050	2.459420	3.442623	4.426230	2.459016	2.459016
T051	6.394491	4.426230	4.426230	2.950820	2.950820
T052	5.902607	5.901639	5.901639	3.442623	3.442623
T053	7.378259	3.442623	3.442623	2.459016	2.459016
T054	3.443187	3.442623	3.934426	1.967213	2.950820
T055	8.362027	8.360656	8.360656	2.459016	2.459016

Table A.8: Frequency estimation results for all patients in the task *Months_backward*.

Patient	Benchmark(Hz)	Euler_phase(Hz)	Euler_gray(Hz)	Lag_with_smooth(Hz)	Lag_no_smooth(Hz)
T001	2.459420	4.426230	3.442623	3.442623	3.442623
T002	4.426955	4.918033	3.934426	7.377049	7.377049
T003	5.902607	10.327869	4.918033	12.295082	12.295082
T005	6.886375	3.934426	0.000000	2.459016	2.459016
T006	6.394491	6.393443	7.377049	10.819672	10.819672
T007	7.378259	4.426230	6.393443	4.918033	4.426230
T008	5.410723	5.409836	5.409836	5.409836	5.409836
T009	6.886375	3.442623	3.442623	1.967213	1.967213
T010	3.935071	3.934426	3.934426	2.459016	2.950820
T011	4.918839	4.918033	4.918033	10.327869	10.327869
T012	4.918839	4.918033	4.918033	4.918033	4.918033
T013	4.918839	4.918033	4.918033	2.459016	2.459016
T014	10.821446	5.409836	5.409836	5.409836	5.409836
T015	6.394491	7.377049	13.770492	14.262295	14.262295
T016	5.902607	12.786885	5.901639	0.000000	0.000000
T017	6.886375	5.409836	3.934426	2.950820	2.950820
T018	3.935071	3.934426	5.901639	5.409836	5.409836
T019	3.443187	3.934426	3.934426	5.409836	5.409836
T020	6.886375	6.885246	5.409836	6.885246	6.885246
T021	2.459420	3.934426	12.295082	2.950820	2.459016
T022	4.426955	4.426230	4.426230	4.918033	4.918033
T023	3.935071	3.934426	3.442623	14.262295	14.262295
T024	4.918839	5.409836	5.409836	5.409836	5.409836
T025	4.426955	4.426230	5.901639	2.950820	2.950820
T026	2.459420	10.327869	10.327869	10.327869	10.327869
T027	6.886375	4.426230	6.885246	3.442623	0.000000
T028	2.459420	3.442623	0.000000	2.950820	2.950820
T029	4.918839	4.426230	4.426230	4.426230	4.426230
T030	4.426955	4.918033	4.918033	3.442623	0.000000
T031	5.410723	5.901639	4.426230	4.426230	4.426230
T032	5.410723	5.409836	5.409836	5.409836	6.393443
T033	5.902607	5.901639	5.901639	5.901639	5.901639
T034	2.951303	3.934426	3.934426	2.459016	2.459016
T036	7.870143	3.442623	3.442623	3.442623	3.442623
T037	2.951303	4.426230	4.918033	14.754098	14.754098
T038	4.426955	2.950820	2.950820	2.950820	3.442623
T039	6.394491	3.934426	3.934426	14.262295	14.262295
T040	2.459420	3.934426	4.426230	1.967213	1.967213
T041	2.459420	3.442623	3.442623	2.459016	2.459016
T042	3.443187	3.442623	3.442623	3.442623	3.442623
T043	5.902607	4.918033	6.885246	2.459016	2.459016
T044	3.443187	3.442623	3.442623	0.000000	0.000000
T045	4.918839	4.918033	4.918033	4.918033	4.918033
T046	6.886375	10.327869	3.442623	6.885246	1.967213
T047	4.918839	3.442623	3.442623	2.950820	2.950820
T050	5.410723	3.934426	8.852459	0.000000	0.000000
T051	5.902607	4.426230	6.885246	6.393443	6.393443
T052	5.902607	5.409836	5.409836	4.918033	4.918033
T053	1.967536	3.442623	3.442623	2.950820	1.967213
T054	7.378259	3.934426	4.918033	3.934426	2.459016
T055	7.870143	7.868852	7.868852	7.868852	7.868852
T035_2	3.443187	4.918033	4.918033	14.754098	14.754098
T035_3	3.935071	5.901639	5.901639	5.901639	5.901639

Table A.9: Frequency estimation results for all patients in the task *Playing_piano*.

Patient	Benchmark(Hz)	Euler_phase(Hz)	Euler_gray(Hz)	Lag_with_smooth(Hz)	Lag_no_smooth(Hz)
T001	2.459420	5.901639	10.819672	2.459016	2.950820
T002	4.918839	3.442623	3.442623	1.967213	1.967213
T003	2.459420	4.426230	4.426230	2.950820	2.459016
T005	5.902607	4.426230	3.934426	3.934426	13.278689
T006	5.902607	5.901639	5.409836	5.409836	5.409836
T007	3.443187	3.442623	3.442623	2.459016	3.442623
T008	5.410723	5.409836	5.409836	5.409836	5.409836
T009	6.394491	3.934426	4.426230	2.459016	8.852459
T010	7.870143	3.934426	4.426230	14.754098	14.754098
T011	5.410723	5.409836	5.409836	2.950820	2.950820
T012	4.918839	4.918033	4.918033	4.918033	4.918033
T013	4.426955	4.426230	4.426230	4.426230	2.950820
T014	5.410723	5.409836	5.409836	5.901639	5.901639
T015	5.410723	5.409836	4.918033	3.934426	3.934426
T016	5.410723	5.409836	5.409836	5.901639	5.901639
T017	3.935071	3.934426	4.426230	3.442623	3.442623
T018	2.951303	4.426230	4.426230	4.426230	2.950820
T019	8.853910	3.442623	3.934426	2.459016	2.459016
T020	6.394491	3.934426	3.934426	14.262295	14.262295
T021	2.459420	4.426230	4.426230	3.442623	3.442623
T022	4.426955	10.819672	7.868852	2.459016	14.262295
T024	5.410723	5.409836	5.409836	5.409836	5.409836
T025	4.426955	3.934426	3.934426	14.262295	14.262295
T026	8.853910	10.327869	10.327869	10.327869	10.327869
T027	1.967536	3.934426	3.934426	2.950820	2.950820
T028	6.394491	3.934426	5.901639	2.950820	2.950820
T029	2.951303	3.442623	3.442623	2.950820	2.950820
T030	4.426955	4.426230	4.426230	4.426230	4.426230
T031	5.902607	3.934426	4.426230	2.459016	1.967213
T032	5.410723	5.409836	5.409836	5.409836	5.409836
T033	5.902607	5.901639	5.901639	5.901639	1.967213
T034	8.853910	3.442623	0.000000	3.934426	3.934426
T035	2.951303	3.442623	3.934426	2.459016	2.459016
T036	7.378259	3.442623	3.442623	2.459016	2.459016
T037	6.886375	3.442623	3.934426	14.754098	14.754098
T038	4.918839	6.885246	6.885246	2.950820	2.950820
T039	4.918839	4.918033	4.918033	4.918033	4.918033
T040	2.459420	3.442623	3.442623	2.950820	3.442623
T041	6.394491	3.934426	4.918033	14.262295	14.262295
T042	5.902607	4.426230	4.918033	3.934426	5.409836
T043	5.410723	5.409836	4.426230	2.459016	2.459016
T044	4.426955	3.442623	3.934426	1.967213	1.967213
T045	5.410723	5.409836	5.409836	5.409836	5.409836
T046	5.410723	10.327869	4.918033	5.409836	5.409836
T047	3.443187	3.934426	3.442623	2.459016	2.459016
T050	6.394491	3.934426	3.934426	2.950820	2.950820
T051	5.902607	4.426230	4.426230	4.426230	1.967213
T052	5.902607	5.901639	5.901639	5.901639	5.901639
T053	2.459420	3.442623	3.442623	2.950820	4.426230
T054	2.951303	3.934426	3.934426	2.950820	2.950820
T055	7.870143	7.868852	7.868852	7.868852	7.868852
T006_2	5.902607	5.901639	5.901639	14.262295	14.262295

Table A.10: Frequency estimation results for all patients in the task *Rest*.

Patient	Benchmark(Hz)	Euler_phase(Hz)	Euler_gray(Hz)	Lag_with_smooth(Hz)	Lag_no_smooth(Hz)
T001	4.426955	4.426230	4.426230	14.262295	14.262295
T002	4.918839	4.426230	4.426230	14.262295	14.262295
T003	5.902607	4.426230	4.426230	2.459016	2.459016
T004	4.918839	4.918033	4.918033	14.262295	14.262295
T005	6.394491	4.918033	4.918033	12.295082	12.295082
T006	5.902607	6.393443	8.852459	4.426230	4.426230
T007	9.345794	9.344262	9.344262	3.442623	3.442623
T008	4.426955	4.426230	4.426230	4.426230	4.426230
T009	5.902607	6.885246	6.885246	11.311475	11.311475
T010	9.345794	3.934426	4.918033	2.950820	2.950820
T011	4.426955	4.426230	4.426230	4.426230	4.426230
T012	4.918839	4.918033	4.918033	4.918033	4.918033
T013	4.426955	5.409836	8.360656	12.295082	12.295082
T014	5.410723	5.409836	5.409836	5.409836	5.409836
T015	5.410723	5.901639	5.901639	4.426230	4.426230
T016	5.902607	12.786885	12.786885	2.950820	2.950820
T017	6.886375	4.918033	4.918033	14.262295	14.262295
T018	7.870143	5.901639	5.901639	2.950820	2.950820
T019	8.362027	4.426230	4.426230	1.967213	1.967213
T020	6.886375	4.426230	4.426230	3.934426	4.426230
T021	6.886375	7.868852	7.377049	2.459016	2.459016
T022	3.935071	3.934426	3.934426	3.934426	3.934426
T023	7.378259	7.868852	7.868852	14.262295	14.262295
T024	4.918839	4.918033	4.918033	4.918033	4.918033
T025	4.426955	3.442623	3.442623	14.262295	14.262295
T026	6.886375	10.327869	10.327869	14.262295	14.262295
T027	6.394491	4.426230	3.934426	2.950820	2.950820
T028	5.902607	3.442623	5.409836	3.442623	3.442623
T029	6.886375	4.426230	4.426230	14.262295	14.262295
T030	4.426955	4.426230	4.426230	3.442623	3.934426
T031	5.902607	5.901639	3.934426	14.262295	14.262295
T032	4.426955	4.426230	4.426230	3.934426	4.426230
T033	4.426955	4.426230	4.426230	3.934426	3.934426
T034	3.935071	3.934426	3.442623	3.442623	3.442623
T035	5.410723	4.426230	13.278689	10.819672	10.819672
T036	6.886375	7.377049	3.934426	14.754098	14.754098
T037	6.394491	3.934426	3.934426	2.459016	1.967213
T038	6.394491	5.409836	11.803279	4.918033	4.918033
T039	5.410723	3.934426	6.885246	4.426230	4.426230
T040	7.378259	4.426230	4.426230	7.377049	7.377049
T041	5.902607	6.393443	4.918033	3.442623	7.377049
T042	5.410723	5.409836	5.409836	5.409836	5.409836
T043	6.394491	3.934426	5.409836	4.426230	4.426230
T044	4.918839	4.918033	4.918033	4.918033	4.918033
T045	5.902607	10.327869	10.327869	14.262295	14.262295
T046	5.902607	10.327869	10.327869	1.967213	2.459016
T047	2.951303	10.327869	3.442623	3.442623	3.934426
T048	3.935071	3.934426	3.934426	3.442623	3.442623
T049	5.902607	3.934426	7.377049	1.967213	2.459016
T050	5.410723	5.409836	11.803279	14.754098	14.262295
T051	5.410723	3.442623	3.442623	2.950820	2.950820
T052	5.902607	3.934426	3.934426	14.262295	14.262295
T053	3.443187	4.426230	5.409836	3.442623	3.442623
T054	4.918839	3.934426	3.442623	14.262295	3.934426
T055	8.362027	8.360656	8.360656	2.950820	2.950820
T006_2	4.918839	4.918033	4.918033	6.885246	6.885246
T041_2	5.410723	3.934426	8.360656	0.000000	7.868852

Table A.11: Frequency estimation results for all patients in the task *Rest_in_supination*.

Patient	Benchmark(Hz)	Euler_phase(Hz)	Euler_gray(Hz)	Lag_with_smooth(Hz)	Lag_no_smooth(Hz)
T010	9.837678	3.442623	9.344262	10.327869	10.327869
T013	4.918839	5.409836	5.409836	13.278689	13.278689
T014	5.410723	5.409836	5.409836	5.901639	5.901639
T015	5.410723	5.901639	5.901639	5.901639	5.901639
T017	6.886375	3.934426	10.819672	9.344262	9.344262
T018	5.410723	4.426230	4.918033	14.754098	14.262295
T019	7.870143	3.934426	11.311475	6.393443	6.393443
T020	6.394491	6.393443	6.393443	14.262295	14.262295
T021	4.426955	6.885246	6.393443	13.770492	14.262295
T022	4.426955	3.934426	3.934426	6.885246	6.885246
T023	8.362027	3.442623	4.918033	2.459016	2.459016
T024	4.918839	5.409836	4.918033	4.918033	5.409836
T025	4.426955	5.901639	10.327869	4.426230	4.426230
T026	8.362027	10.327869	10.327869	2.459016	2.459016
T027	5.410723	5.409836	6.393443	14.754098	14.754098
T028	3.443187	3.934426	8.852459	4.426230	4.426230
T029	8.853910	4.426230	4.426230	2.459016	2.459016
T030	3.935071	4.918033	4.918033	2.459016	2.459016
T031	5.902607	8.360656	8.360656	14.262295	1.967213
T032	4.918839	4.918033	4.918033	4.918033	4.918033
T033	5.902607	5.901639	5.901639	2.459016	2.459016
T034	3.935071	3.442623	3.442623	1.967213	1.967213
T035	4.918839	3.934426	3.934426	11.311475	14.262295
T036	7.378259	5.409836	5.409836	3.442623	3.442623
T037	6.886375	3.934426	3.934426	2.459016	2.459016
T038	4.426955	3.934426	3.934426	2.950820	2.459016
T039	5.902607	3.934426	5.901639	1.967213	1.967213
T040	3.935071	4.918033	4.918033	2.459016	2.459016
T041	7.378259	4.918033	5.409836	3.442623	3.442623
T042	3.935071	3.934426	3.934426	2.950820	14.262295
T043	5.410723	3.442623	4.426230	2.459016	2.459016
T044	4.426955	4.426230	4.426230	4.426230	4.426230
T045	5.902607	10.327869	4.918033	5.901639	14.262295
T046	5.410723	10.327869	10.327869	9.836066	9.836066
T047	7.378259	10.327869	5.409836	2.459016	7.377049
T048	5.410723	10.327869	10.327869	10.327869	10.327869
T049	6.394491	3.934426	4.918033	2.459016	2.459016
T050	6.394491	4.918033	4.918033	14.262295	14.262295
T051	6.886375	5.901639	5.901639	5.901639	5.901639
T052	5.902607	6.393443	6.393443	5.409836	5.409836
T053	3.443187	3.934426	6.393443	1.967213	1.967213
T054	4.918839	4.426230	4.426230	3.442623	3.442623
T055	7.870143	8.360656	8.360656	14.262295	14.262295
T002_2	4.426955	4.426230	4.426230	4.426230	4.426230

Table A.12: Frequency estimation results for all patients in the task *Spiral_left*.

Patient	Benchmark(Hz)	Euler_phase(Hz)	Euler_gray(Hz)	Lag_with_smooth(Hz)	Lag_no_smooth(Hz)
T001	7.378259	4.426230	4.426230	2.950820	2.950820
T002	4.918839	3.934426	3.934426	14.262295	14.262295
T003	1.967536	5.901639	5.409836	2.950820	2.950820
T005	7.870143	3.934426	12.786885	2.950820	2.950820
T007	2.459420	4.426230	3.934426	14.754098	14.754098
T018	6.886375	5.901639	5.901639	5.901639	5.901639
T019	7.870143	3.934426	3.934426	1.967213	1.967213
T029	2.459420	3.934426	4.918033	2.950820	2.950820
T030	4.918839	3.934426	3.934426	2.950820	2.950820
T032	5.902607	3.442623	5.409836	2.459016	2.459016
T038	2.459420	4.426230	4.426230	2.459016	2.459016
T040	4.426955	3.934426	3.934426	2.950820	2.950820
T043	5.410723	3.442623	3.442623	1.967213	1.967213
T044	4.426955	4.426230	4.918033	2.459016	2.459016
T046	4.918839	10.327869	4.918033	2.950820	2.950820
T048	2.951303	3.442623	3.442623	2.459016	2.459016
T050	5.410723	4.426230	4.426230	3.442623	3.442623
T055	8.853910	3.442623	3.934426	2.459016	2.459016

Table A.13: Frequency estimation results for all patients in the task *Spiral_right*.

Patient	Benchmark(Hz)	Euler_phase(Hz)	Euler_gray(Hz)	Lag_with_smooth(Hz)	Lag_no_smooth(Hz)
T001	6.394491	3.442623	8.360656	3.934426	3.442623
T002	7.378259	3.442623	3.442623	1.475410	1.475410
T003	6.394491	8.852459	0.000000	3.934426	3.442623
T005	7.378259	4.426230	4.426230	7.377049	7.377049
T018	4.918839	3.442623	3.934426	1.967213	1.967213
T019	9.345794	4.426230	0.000000	4.426230	4.426230
T021	2.951303	3.442623	0.000000	2.950820	2.459016
T022	2.459420	4.426230	5.901639	2.459016	2.459016
T026	2.951303	3.442623	3.934426	2.459016	2.459016
T029	3.935071	3.934426	3.934426	1.967213	1.967213
T031	1.967536	3.934426	3.934426	2.459016	2.459016
T032	4.426955	4.426230	4.426230	1.967213	1.967213
T034	8.853910	3.442623	3.442623	2.459016	2.459016
T036	6.886375	3.934426	3.934426	1.967213	1.967213
T038	7.378259	3.934426	3.934426	2.459016	1.967213
T039	3.935071	3.934426	3.934426	14.754098	14.754098
T040	3.935071	5.901639	5.901639	2.459016	2.459016
T042	6.394491	3.934426	3.934426	2.459016	2.459016
T044	4.918839	4.426230	3.442623	2.950820	2.459016
T046	6.394491	3.442623	4.426230	2.950820	2.950820
T050	5.902607	3.934426	3.934426	2.950820	2.950820
T055	9.837678	3.442623	0.000000	3.934426	3.934426

Table A.14: Frequency estimation results for all patients in the task *Thumps_up*.

Patient	Benchmark(Hz)	Euler_phase(Hz)	Euler_gray(Hz)	Lag_with_smooth(Hz)	Lag_no_smooth(Hz)
T001	6.886375	3.442623	0.000000	2.950820	2.950820
T002	4.918839	4.426230	4.426230	4.426230	4.426230
T003	5.410723	3.442623	3.442623	3.442623	7.868852
T004	4.918839	3.442623	6.393443	2.950820	2.950820
T005	6.394491	8.360656	5.901639	2.950820	2.950820
T006	6.394491	4.426230	11.311475	8.360656	8.360656
T007	2.459420	7.868852	7.868852	2.950820	2.950820
T008	4.918839	5.409836	5.409836	5.409836	5.409836
T009	6.886375	7.868852	10.327869	2.459016	11.311475
T010	8.853910	8.360656	3.934426	2.459016	2.459016
T011	4.918839	4.918033	4.918033	4.918033	4.918033
T012	7.378259	7.868852	9.344262	2.950820	2.950820
T013	4.426955	3.934426	4.918033	4.426230	4.426230
T014	5.410723	5.409836	5.409836	5.409836	5.409836
T015	6.886375	3.934426	3.934426	6.885246	6.393443
T016	5.902607	6.885246	4.918033	2.459016	2.459016
T017	6.886375	5.901639	5.901639	7.377049	7.377049
T018	9.345794	4.918033	4.918033	2.459016	2.459016
T019	9.345794	5.901639	5.901639	2.459016	2.459016
T020	2.459420	3.442623	3.442623	2.459016	2.459016
T021	1.967536	3.442623	8.360656	2.950820	2.950820
T022	2.459420	4.426230	4.918033	2.459016	2.459016
T023	11.805214	3.442623	3.934426	2.459016	2.459016
T024	5.410723	5.409836	5.409836	5.409836	5.409836
T026	9.345794	10.327869	9.836066	14.262295	14.262295
T027	4.918839	4.918033	4.918033	4.918033	4.918033
T028	2.459420	8.360656	8.360656	2.459016	2.459016
T029	4.426955	4.426230	4.426230	3.934426	3.934426
T030	4.426955	3.442623	3.442623	2.950820	2.950820
T031	5.902607	5.901639	5.901639	2.459016	2.950820
T032	5.410723	4.426230	3.442623	2.459016	2.459016
T033	5.902607	5.901639	5.901639	5.901639	5.901639
T034	2.951303	3.442623	3.934426	3.442623	3.442623
T035	5.902607	3.934426	7.377049	2.459016	2.459016
T036	2.459420	5.409836	5.409836	13.770492	2.459016
T037	6.394491	5.901639	3.934426	2.459016	2.950820
T038	6.394491	5.409836	5.901639	3.934426	1.967213
T039	4.918839	4.918033	4.918033	2.950820	2.950820
T040	2.459420	7.377049	4.426230	2.950820	2.950820
T041	8.362027	4.918033	7.868852	4.918033	4.918033
T042	5.410723	5.409836	5.409836	6.885246	6.885246
T043	5.902607	7.377049	7.377049	2.459016	2.459016
T044	4.426955	4.426230	4.426230	4.426230	4.426230
T045	4.918839	4.918033	4.918033	4.918033	4.918033
T046	6.394491	4.426230	4.426230	2.459016	2.459016
T047	2.459420	3.934426	3.934426	1.967213	1.967213
T048	2.951303	10.327869	6.885246	14.262295	14.262295
T049	6.394491	3.442623	3.934426	4.426230	4.426230
T050	5.410723	3.442623	3.442623	3.442623	3.442623
T051	6.886375	3.934426	5.901639	2.950820	2.950820
T052	5.410723	5.901639	5.409836	4.426230	4.426230
T053	2.459420	3.934426	3.934426	1.967213	1.967213
T054	6.394491	5.901639	5.901639	2.950820	2.459016
T055	8.853910	8.852459	8.852459	2.459016	2.459016

Table A.15: Frequency estimation results for all patients in the task *Top_nose_left*.

Patient	Benchmark(Hz)	Euler_phase(Hz)	Euler_gray(Hz)	Lag_with_smooth(Hz)	Lag_no_smooth(Hz)
T001	2.459420	6.393443	4.918033	4.918033	4.918033
T002	5.902607	4.426230	4.426230	2.459016	3.442623
T003	2.459420	10.819672	10.819672	0.000000	0.000000
T004	6.394491	2.950820	2.950820	2.950820	2.950820
T005	7.870143	0.000000	0.000000	2.459016	1.475410
T006	4.918839	4.918033	6.393443	0.000000	0.000000
T007	2.459420	0.000000	0.000000	1.967213	1.967213
T008	6.394491	5.901639	0.000000	1.967213	1.967213
T009	5.410723	8.852459	2.950820	2.950820	2.950820
T010	11.805214	3.442623	0.000000	1.967213	1.967213
T011	5.410723	3.442623	5.409836	2.459016	2.459016
T012	4.426955	7.377049	7.377049	7.377049	7.377049
T013	4.918839	5.409836	5.409836	3.934426	3.934426
T014	4.426955	3.442623	0.000000	1.475410	1.475410
T015	5.902607	5.901639	5.409836	13.770492	13.770492
T016	5.902607	6.393443	6.393443	6.393443	6.393443
T017	2.459420	3.442623	3.442623	2.459016	2.459016
T018	7.870143	6.885246	6.885246	6.393443	6.393443
T019	2.951303	4.426230	4.426230	2.459016	2.459016
T020	2.951303	3.934426	3.934426	2.459016	2.459016
T021	3.935071	3.442623	6.393443	2.459016	2.459016
T022	2.459420	3.442623	0.000000	1.967213	1.967213
T023	8.853910	8.852459	4.918033	0.000000	3.442623
T024	2.459420	3.442623	2.950820	6.885246	6.885246
T026	2.951303	3.442623	0.000000	14.262295	14.262295
T027	5.410723	3.934426	0.000000	1.967213	1.967213
T035	2.951303	9.836066	8.852459	3.442623	3.442623
T036	2.951303	3.442623	3.442623	0.000000	0.000000
T037	2.951303	3.934426	4.426230	1.967213	1.967213
T038	5.410723	3.442623	3.442623	0.000000	3.934426
T039	2.951303	3.442623	0.000000	1.967213	1.967213
T040	2.459420	3.442623	0.000000	2.459016	2.459016
T041	3.935071	3.934426	10.327869	2.459016	0.000000
T042	1.967536	5.409836	5.409836	2.459016	2.459016
T043	2.459420	3.934426	4.918033	2.950820	1.967213
T044	4.426955	3.934426	4.426230	14.262295	14.262295
T045	5.410723	10.819672	10.819672	3.934426	2.950820
T046	4.918839	11.803279	10.327869	2.950820	2.950820
T047	3.443187	4.918033	4.426230	2.459016	2.459016
T048	2.459420	3.934426	0.000000	2.950820	1.967213
T050	6.886375	3.934426	5.901639	2.950820	2.950820
T051	1.967536	3.442623	3.934426	2.950820	2.950820
T052	6.886375	8.360656	8.360656	1.967213	1.967213
T053	5.410723	4.918033	4.918033	1.967213	1.967213
T054	1.967536	3.442623	12.786885	2.950820	2.950820
T055	8.362027	8.852459	3.442623	2.950820	2.950820
T011_2	4.918839	3.442623	0.000000	1.967213	2.950820

Table A.16: Frequency estimation results for all patients in the task *Top_nose_right*.

Patient	Benchmark(Hz)	Euler_phase(Hz)	Euler_gray(Hz)	Lag_with_smooth(Hz)	Lag_no_smooth(Hz)
T001	7.378259	3.442623	0.000000	1.967213	1.967213
T002	5.410723	3.442623	0.000000	1.967213	1.967213
T003	5.410723	3.442623	0.000000	2.459016	2.459016
T004	4.918839	3.442623	0.000000	2.459016	1.967213
T005	3.935071	5.901639	6.393443	0.000000	0.000000
T006	6.886375	3.934426	0.000000	1.475410	1.967213
T007	3.443187	4.426230	4.426230	0.000000	0.000000
T008	4.918839	3.934426	5.409836	4.918033	4.918033
T009	2.459420	3.934426	0.000000	2.459016	1.967213
T010	3.443187	3.934426	3.934426	0.000000	0.000000
T011	5.410723	4.918033	8.852459	5.409836	5.409836
T012	7.870143	3.442623	0.000000	1.967213	1.967213
T013	5.410723	3.442623	3.934426	2.459016	1.967213
T014	5.410723	5.901639	5.901639	5.409836	5.409836
T015	1.967536	3.442623	0.000000	1.967213	1.967213
T016	6.394491	4.426230	0.000000	1.967213	1.967213
T017	4.426955	3.934426	3.934426	2.459016	2.459016
T018	2.459420	3.442623	0.000000	3.934426	3.934426
T019	1.967536	2.950820	0.000000	1.967213	1.967213
T020	2.459420	3.934426	0.000000	2.459016	2.459016
T021	6.886375	3.442623	3.442623	2.459016	2.459016
T022	4.426955	12.786885	12.786885	0.000000	0.000000
T023	6.886375	4.918033	4.918033	14.754098	14.754098
T024	4.918839	3.934426	4.918033	2.950820	2.950820
T026	1.967536	2.950820	4.426230	1.475410	1.475410
T027	2.951303	3.934426	3.934426	3.442623	2.950820
T028	3.443187	8.852459	3.934426	2.950820	2.950820
T029	1.967536	3.934426	0.000000	1.967213	1.967213
T030	3.935071	3.442623	6.393443	3.442623	3.442623
T031	2.459420	4.426230	0.000000	2.459016	2.459016
T032	4.918839	4.918033	4.426230	2.950820	2.950820
T033	6.394491	3.442623	3.934426	1.967213	2.459016
T034	2.459420	3.934426	0.000000	1.967213	1.967213
T035	2.459420	3.934426	0.000000	2.459016	2.459016
T036	2.459420	3.442623	3.442623	2.459016	2.459016
T037	3.443187	3.934426	3.934426	2.950820	2.950820
T038	6.886375	3.442623	0.000000	1.967213	1.967213
T039	5.902607	3.442623	12.295082	2.459016	2.459016
T040	3.443187	5.409836	5.409836	2.950820	2.950820
T041	6.886375	3.442623	0.000000	1.967213	1.967213
T042	5.902607	3.442623	0.000000	2.459016	2.459016
T043	3.443187	3.442623	5.409836	2.459016	2.459016
T044	4.918839	3.934426	0.000000	2.459016	2.459016
T045	4.426955	3.934426	0.000000	1.967213	1.967213
T046	2.459420	3.442623	0.000000	2.459016	2.459016
T047	10.329562	3.934426	0.000000	1.967213	1.967213
T048	2.951303	8.360656	8.360656	2.459016	2.459016
T050	2.951303	3.442623	3.442623	1.967213	1.967213
T051	8.853910	3.442623	3.934426	2.459016	2.459016
T052	6.394491	3.442623	0.000000	2.459016	2.459016
T053	2.459420	0.000000	0.000000	2.459016	2.459016
T054	7.378259	4.426230	4.918033	2.459016	1.967213
T055	7.870143	2.950820	0.000000	5.901639	1.967213
T011_2	5.410723	5.901639	6.393443	2.459016	1.967213

Table A.17: Frequency estimation results for all patients in the task *Top_top*.

Patient	Benchmark(Hz)	Euler_phase(Hz)	Euler_gray(Hz)	Lag_with_smooth(Hz)	Lag_no_smooth(Hz)
T001	3.935071	4.918033	10.327869	2.950820	2.950820
T002	4.426955	3.442623	3.934426	3.442623	3.442623
T003	5.902607	3.934426	11.311475	2.950820	2.950820
T004	4.918839	10.819672	10.819672	8.360656	8.360656
T005	6.394491	4.918033	6.393443	2.950820	2.950820
T006	5.902607	5.901639	5.901639	1.967213	1.967213
T007	8.362027	3.442623	4.426230	13.278689	1.967213
T008	4.918839	5.409836	5.409836	5.409836	5.409836
T009	5.902607	6.393443	4.918033	3.442623	3.442623
T010	8.362027	3.442623	5.409836	1.967213	1.967213
T011	4.918839	5.409836	5.409836	5.409836	5.409836
T012	4.918839	4.918033	4.918033	4.918033	4.918033
T013	4.918839	4.918033	4.918033	2.950820	2.950820
T014	5.410723	5.901639	5.901639	5.901639	5.409836
T015	6.394491	7.377049	7.377049	6.885246	7.868852
T016	5.902607	5.901639	5.901639	5.901639	5.901639
T017	3.443187	5.901639	4.918033	2.950820	2.459016
T018	3.443187	7.868852	6.393443	3.442623	4.426230
T019	4.918839	3.934426	3.934426	2.950820	2.950820
T020	2.459420	4.426230	4.426230	2.459016	2.459016
T021	5.902607	6.885246	9.836066	2.459016	1.967213
T022	4.918839	4.918033	4.918033	4.918033	4.918033
T023	8.362027	5.901639	4.918033	2.459016	2.459016
T024	5.410723	5.409836	5.409836	5.409836	5.409836
T026	3.935071	10.327869	10.327869	4.426230	2.950820
T027	4.918839	4.918033	4.918033	2.459016	2.459016
T028	5.902607	4.918033	5.901639	2.950820	2.950820
T029	2.459420	4.426230	4.426230	2.459016	2.459016
T030	4.426955	4.426230	4.426230	2.950820	2.950820
T031	5.902607	5.901639	5.901639	1.967213	5.901639
T032	5.410723	5.409836	5.409836	5.409836	5.409836
T033	2.951303	5.901639	6.393443	2.459016	2.459016
T034	7.870143	3.442623	3.442623	2.459016	2.459016
T035	3.935071	3.934426	4.426230	2.459016	2.459016
T036	7.378259	5.901639	5.901639	2.950820	5.901639
T037	6.886375	4.918033	7.377049	2.459016	2.459016
T038	3.935071	4.426230	4.426230	4.918033	4.918033
T039	4.918839	5.409836	5.409836	5.409836	4.918033
T040	3.443187	3.934426	4.426230	2.459016	2.459016
T041	6.394491	6.393443	4.426230	4.918033	4.426230
T042	5.410723	5.409836	5.409836	5.409836	5.409836
T043	6.886375	5.409836	5.409836	10.819672	5.901639
T044	4.426955	4.426230	4.426230	4.426230	4.426230
T045	4.918839	4.918033	4.918033	4.918033	4.918033
T046	6.394491	10.327869	10.327869	4.918033	4.918033
T047	3.443187	3.442623	3.442623	14.754098	14.754098
T048	3.443187	10.327869	4.426230	2.950820	2.950820
T049	5.902607	5.409836	3.934426	2.950820	2.950820
T050	5.410723	6.393443	6.393443	14.262295	14.262295
T051	5.902607	4.426230	6.393443	2.950820	5.901639
T052	6.394491	6.393443	5.409836	3.442623	1.967213
T053	2.951303	5.901639	4.426230	14.262295	14.262295
T054	5.410723	3.934426	5.409836	2.459016	1.967213
T055	8.853910	9.344262	9.344262	2.950820	2.950820

Table A.18: Frequency estimation results for all patients in the task *Weight*.

Patient	Benchmark(Hz)	Euler_phase(Hz)	Euler_gray(Hz)	Lag_with_smooth(Hz)	Lag_no_smooth(Hz)
T001	6.394491	4.426230	13.278689	3.442623	3.442623
T002	4.426955	4.426230	4.426230	3.934426	3.934426
T003	4.918839	4.918033	4.918033	2.459016	2.459016
T005	7.378259	8.852459	7.868852	0.000000	0.000000
T006	6.394491	6.393443	6.885246	4.426230	3.442623
T007	2.459420	4.426230	4.426230	2.950820	3.442623
T009	6.886375	4.918033	7.868852	14.262295	14.262295
T010	10.329562	3.442623	5.409836	14.262295	14.262295
T011	4.918839	4.918033	4.918033	14.262295	14.262295
T012	6.886375	5.409836	4.426230	2.950820	2.950820
T014	5.902607	6.393443	6.393443	3.934426	5.901639
T015	5.410723	5.409836	5.409836	14.262295	14.262295
T016	6.394491	6.393443	6.393443	2.459016	2.459016
T017	2.951303	4.918033	3.934426	4.426230	4.426230
T018	3.443187	3.934426	3.934426	2.950820	3.442623
T019	4.918839	3.934426	3.934426	2.950820	2.950820
T021	7.870143	4.426230	3.934426	3.442623	14.262295
T022	2.459420	3.934426	3.934426	4.918033	4.918033
T023	4.426955	4.918033	4.918033	14.262295	14.262295
T024	4.918839	3.442623	3.934426	2.950820	2.950820
T026	8.853910	4.918033	3.442623	3.442623	3.442623
T027	4.918839	3.442623	3.934426	2.459016	2.459016
T028	8.362027	3.442623	7.868852	10.327869	2.950820
T029	4.426955	4.426230	4.426230	4.426230	4.426230
T030	4.426955	4.426230	4.426230	2.459016	2.459016
T031	5.902607	3.442623	5.409836	14.262295	14.262295
T032	5.902607	4.918033	4.918033	1.967213	2.459016
T033	5.902607	5.901639	5.409836	5.901639	5.901639
T034	4.918839	3.934426	3.442623	2.459016	2.459016
T035	4.426955	9.344262	9.344262	3.442623	3.442623
T036	7.870143	3.934426	9.836066	2.459016	2.459016
T037	6.394491	3.934426	3.934426	2.459016	2.459016
T038	6.886375	3.934426	3.934426	1.967213	2.950820
T039	5.410723	3.934426	3.934426	3.934426	5.409836
T040	10.329562	3.442623	3.442623	2.950820	2.950820
T041	6.886375	5.409836	4.426230	2.459016	2.459016
T042	6.394491	5.901639	0.000000	3.442623	3.442623
T043	6.394491	3.934426	5.409836	4.918033	4.918033
T044	6.394491	6.393443	4.918033	2.459016	2.459016
T045	4.918839	4.918033	4.918033	4.918033	4.918033
T046	6.394491	10.327869	4.426230	7.377049	7.377049
T047	9.345794	10.327869	6.885246	1.967213	1.967213
T050	6.886375	4.426230	10.327869	2.459016	2.459016
T051	7.870143	4.426230	3.442623	6.393443	6.393443
T052	6.394491	6.393443	6.393443	6.393443	6.393443
T053	2.459420	3.934426	4.426230	1.967213	1.967213
T054	4.426955	3.934426	3.934426	2.459016	2.459016
T055	8.362027	8.852459	8.852459	2.459016	2.459016
T038_2	5.410723	4.918033	4.918033	2.950820	0.000000

Table A.19: Frequency estimation results for all patients in the task *Writing_left*.

Patient	Benchmark(Hz)	Euler_phase(Hz)	Euler_gray(Hz)	Lag_with_smooth(Hz)	Lag_no_smooth(Hz)
T001	7.378259	3.442623	3.442623	2.459016	3.442623
T002	4.918839	6.393443	6.393443	7.868852	2.950820
T003	5.902607	5.901639	5.901639	3.442623	3.442623
T005	6.886375	4.426230	4.426230	14.262295	3.442623
T007	5.410723	5.901639	5.901639	2.459016	2.459016
T010	4.426955	3.934426	3.934426	2.459016	2.459016
T012	4.918839	4.918033	4.918033	4.918033	2.459016
T013	4.426955	4.426230	4.426230	4.426230	3.442623
T018	7.870143	5.901639	5.901639	3.442623	2.459016
T019	8.853910	3.442623	3.442623	1.967213	2.950820
T020	7.870143	5.901639	4.426230	2.950820	14.754098
T021	2.459420	3.934426	3.934426	2.950820	2.459016
T022	2.459420	4.426230	4.426230	3.934426	2.459016
T029	2.951303	3.442623	3.442623	3.442623	2.950820
T030	4.918839	4.918033	4.918033	1.967213	2.459016
T031	5.902607	3.934426	3.934426	2.459016	2.459016
T032	5.410723	3.934426	3.934426	3.442623	3.442623
T034	5.902607	3.442623	4.426230	3.442623	2.459016
T035	6.394491	3.934426	4.918033	2.950820	2.459016
T036	7.870143	7.377049	7.377049	2.459016	2.950820
T038	5.902607	5.409836	4.426230	14.262295	2.459016
T039	5.902607	4.918033	4.918033	2.459016	2.459016
T040	3.935071	4.918033	7.868852	14.262295	14.262295
T041	6.886375	4.426230	4.426230	2.950820	2.950820
T042	5.410723	5.409836	5.409836	14.262295	2.459016
T043	2.459420	3.934426	3.934426	3.934426	2.459016
T044	4.426955	4.918033	3.934426	2.459016	2.950820
T045	5.410723	5.901639	5.901639	2.950820	2.459016
T048	3.443187	3.934426	3.934426	1.967213	2.459016
T050	5.902607	3.934426	3.934426	2.459016	2.459016
T051	9.837678	4.918033	4.918033	5.901639	2.950820
T053	3.935071	3.934426	4.918033	2.950820	2.950820
T055	9.837678	5.409836	5.409836	2.459016	2.950820

Table A.20: Frequency estimation results for all patients in the task *Writing_right*.

Patient	Benchmark(Hz)	Euler_phase(Hz)	Euler_gray(Hz)	Lag_with_smooth(Hz)	Lag_no_smooth(Hz)
T001	6.886375	4.426230	4.918033	2.459016	2.459016
T002	1.967536	4.426230	4.426230	1.967213	1.967213
T003	6.394491	6.393443	6.393443	2.950820	2.950820
T005	5.902607	3.934426	4.918033	2.950820	3.934426
T007	4.918839	5.409836	4.918033	4.426230	4.426230
T010	8.853910	4.426230	5.409836	2.459016	5.901639
T012	6.886375	3.934426	4.918033	2.459016	2.459016
T013	5.410723	3.934426	3.934426	5.901639	5.901639
T018	5.902607	3.442623	4.426230	2.950820	2.950820
T019	5.410723	3.934426	3.934426	2.459016	2.459016
T020	2.459420	4.918033	4.918033	2.459016	2.459016
T021	6.394491	3.442623	4.918033	2.459016	2.459016
T022	3.935071	3.934426	6.393443	14.754098	14.262295
T026	4.918839	3.934426	4.918033	1.967213	1.967213
T029	5.410723	4.426230	4.426230	2.459016	2.459016
T030	4.426955	4.426230	4.426230	2.459016	2.459016
T031	2.951303	3.442623	4.918033	2.950820	2.950820
T032	4.918839	4.426230	4.426230	1.967213	1.967213
T033	5.410723	4.426230	4.426230	1.967213	1.967213
T034	9.345794	3.934426	3.934426	2.459016	2.459016
T035	5.902607	3.934426	4.426230	2.950820	2.950820
T036	2.459420	3.442623	4.918033	1.967213	1.967213
T038	3.935071	3.934426	4.426230	2.459016	3.442623
T039	4.918839	4.918033	4.918033	2.459016	2.459016
T040	3.443187	3.442623	3.934426	2.950820	2.950820
T041	6.394491	6.393443	6.393443	2.459016	2.459016
T042	6.394491	3.442623	4.426230	3.442623	2.950820
T043	5.902607	4.918033	4.918033	5.409836	5.409836
T044	3.935071	3.934426	4.918033	2.459016	2.459016
T045	5.902607	10.327869	5.901639	2.459016	2.459016
T046	6.394491	4.918033	4.918033	2.459016	2.459016
T048	2.459420	10.327869	10.327869	2.459016	2.459016
T050	5.902607	5.409836	5.901639	2.950820	2.950820
T051	4.426955	4.426230	4.426230	2.459016	2.950820
T053	2.951303	3.442623	4.918033	2.950820	2.950820
T055	7.378259	3.934426	3.934426	2.459016	2.459016
T026_2	2.951303	4.426230	4.918033	1.967213	1.967213

Table A.21: Frequency estimation results for all patients in the task *Extra_writing*.

Patient	Benchmark(Hz)	Euler_phase(Hz)	Euler_gray(Hz)	Lag_with_smooth(Hz)	Lag_no_smooth(Hz)
T039_1	2.459420	3.442623	3.934426	2.459016	2.459016
T039_2	4.426955	3.934426	5.409836	4.426230	4.426230
T010	5.410723	4.918033	9.836066	2.459016	2.459016
T007	3.443187	3.934426	3.934426	2.459016	2.459016
T039_3	6.394491	6.393443	3.442623	2.950820	2.459016